Accepted Manuscript

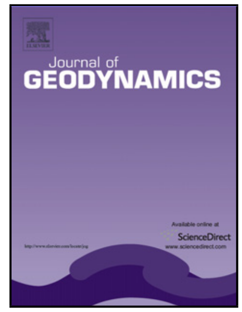

Title: New evidence about the subduction of the Copiapó ridge beneath South America, and its connection with the Chilean-Pampean flat slab, tracked by satellite GOCE and EGM2008 models

Author: Orlando Alvarez Mario Gimenez Andres Folguera Silvana Spagnotto Emilce Bustos Walter Baez Carla Braitenberg

PII: S0264-3707(15)30002-8
DOI: http://dx.doi.org/doi:10.1016/j.jog.2015.08.002
Reference: GEOD 1382

To appear in: *Journal of Geodynamics*

Received date: 30-8-2014
Revised date: 11-8-2015
Accepted date: 12-8-2015

Please cite this article as: Alvarez, O., Gimenez, M., Folguera, A., Spagnotto, S., Bustos, E., Baez, W., Braitenberg, C.,New evidence about the subduction of the Copiapó ridge beneath South America, and its connection with the Chilean-Pampean flat slab, tracked by satellite GOCE and EGM2008 models, *Journal of Geodynamics* (2015), http://dx.doi.org/10.1016/j.jog.2015.08.002

New evidence about the subduction of the Copiapó ridge beneath South America, and its connection with the Chilean-Pampean flat slab, tracked by satellite GOCE and EGM2008 models

Orlando Alvarez[1,2] orlando_a_p@yahoo.com.ar, Mario Gimenez[1,2] gimmario@gmail.com, Andres Folguera[3,2] andresfolguera2@yahoo.com.ar, Silvana Spagnotto [4,2] pampa113@gmail.com, Emilce Bustos[5] emilcebustos@gmail.com, Walter Baez[5] focobaez@hotmail.com, and Carla Braitenberg[6] berg@units.it

[1]*Instituto Geofísico y Sismológico Ing. Volponi, Universidad Nacional de San Juan, Ruta 12, Km 17, CP 5407, San Juan, Argentina.*

[2]*Consejo Nacional de Investigaciones Cientificas y Tecnologicas, CONICET, Argentina.*

[3]*IDEAN - Instituto de Estudios Andinos "Don Pablo Groeber". Departamento de Cs. Geológicas - FCEN - Pab. II. Universidad de Buenos Aires.*

[4]*Depto de Física - Universidad Nacional de San Luis. San Luis, Argentina.*

[5]*INENCO-CONICET. UNSa. Av. Bolivia 5150. CP 4400 Salta.*

[6]*Dipartimento di Matematica e Geoscienze, Universita di Trieste, Via Weiss 1, 34100 Trieste, Italy.*

Corresponding Author: Orlando Alvarez

Postal Address: Mariano Moreno 240(S) dpto:6. Rivadavia, San Juan, Argentina.

Phone: +0054-0264-4267371

ABSTRACT

Satellite-only gravity measurements and those integrated with terrestrial observations provide global gravity field models of unprecedented precision and spatial resolution, ~~which allow analyzing lithospheric structure~~ allowing the analysis of the lithospheric structure. We used the model EGM2008 (Earth Gravitational Model) to calculate the gravity anomaly and the vertical gravity gradient in the South Central Andes region, correcting these quantities by the topographic effect. Both quantities show a spatial relationship between the projected subduction of the Copiapó aseismic ridge (located at about 27º 30’ S), its potential deformational effects in the overriding plate, and the Ojos del Salado-San Buenaventura volcanic lineament. This volcanic lineament constitutes a projection of the volcanic arc towards the retroarc zone, whose origin and development were not clearly understood. The analysis of the gravity anomalies, at the extrapolated zone of the Copiapó ridge beneath the continent, shows a change in the general NNE-trend of the Andean structures to an ENE-direction coincident with the area of the Ojos del Salado-San Buenaventura volcanic lineament. This anomalous pattern over the upper plate is interpreted to be linked with the subduction of the Copiapó ridge.

We explore the relation between deformational effects and volcanism at the northern Chilean-Pampean flat slab and the collision of the Copiapó ridge, on the basis of the

Moho geometry and elastic thicknesses calculated from the new satellite GOCE data. Neotectonic deformations interpreted in previous works associated with volcanic eruptions along the Ojos del Salado-San Buenaventura volcanic lineament is interpreted as caused by crustal doming, imprinted by the subduction of the Copiapó ridge, evidenced by crustal thickening at the sites of ridge inception along the trench.

Finally, we propose that the Copiapó ridge could have controlled the northern edge of the Chilean-Pampean flat slab, due to higher buoyancy, similarly to the control that the Juan Fernandez ridge exerts in the geometry of the flat slab further south.

Keywords: GOCE; Vertical Gravity Gradient; Ojos del Salado-San Buenaventura Lineament; Copiapó aseismic ridge; Chilean-Pampean flat slab.

1. INTRODUCTION

The Andes are the largest active orogenic system developed by subduction of oceanic lithosphere. This continuous and complex mountain belt is the expression of deformational and magmatic processes that acted together with variable intensity along the plate margin. A variable obliquity of the relative convergence between the converging plates, spatio-temporal variable segments of flattenings and steepenings of the subduction zone, delamination phenomena, pluvial gradients and local sites of accretion of oceanic features have determined a strong segmentation of the mountain morphology (Fig. 1) (Gutscher et al. 2000; James and Sacks, 1999; Kay and Coira, 2009; Lamb and Davis, 2003; Martinod et al. 2010; Ramos, 2009).

Among these controls, shallow to flat subduction settings are of special interest since they coincide with segments of high mountains and high orogenic amplitude. These occur at about 10% of the modern convergent margins (Gutscher et al. 2000) and are commonly associated with subduction of overthickened and therefore abnormally buoyant oceanic crust, in oceanic plateaus, seamounts, and aseismic ridges. In particular, the last are considered the major factor associated with the development of shallow subduction configurations in the Andes (Cloos, 1992; Scholtz and Small, 1997; Yañez et al. 2001; Yañez and Cembrano, 2004).

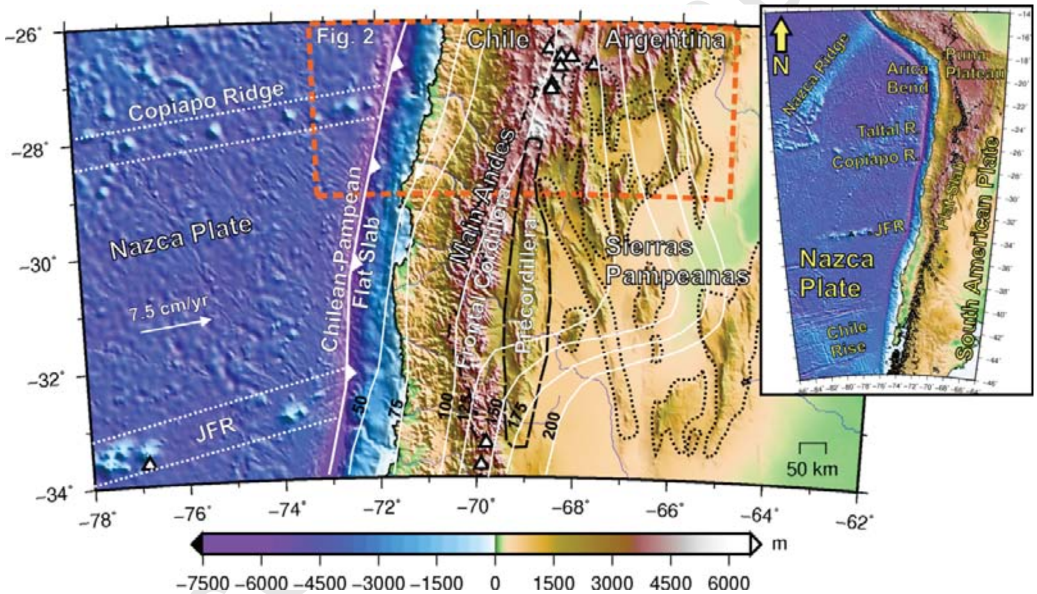

Figure 1. *Shaded digital elevation model of the Southern Central Andes region with superimposed contours of the Wadati-Benioff zone at 25 km intervals (white solid line) describing the Chilean-Pampean flat slab region (Mulcahy et al. 2014). The Precordillera~~, depicted by a~~ (black dashed line) and the Sierras Pampeanas broken foreland~~, by a~~ (black dotted line), are mountain systems associated with the development of the flat slab in the last 17 My. Triangles indicate the current position of the active volcanic arc beyond the limits of the*

flat slab (Siebert and Simkin, 2002). An arc gap is associated with the area of shallowing of the subducted Nazca plate at these latitudes. The Juan Fernandez (JFR) and the Copiapó ridges are indicated (white dotted lines) colliding against the Chilean trench at the southern and northern edges of the flat slab respectively. Nazca–South American plates convergence rate and azimuth (white arrow) is from DeMets et al. (2010).

~~Modern magnitudes of shallow subduction zones are strikingly variable worldwide, being the largest and with greater deformational effects located in the Andes (James and Sacks, 1999; Kay and Coira, 2009; Ramos and Folguera, 2009). Barazangi and Isacks (1976, 1979) related two of the four arc gaps along the Andes to flat-slab subduction settings based on location of earthquake´s hypocenters. In their analysis, the Peru (3ºS to 15ºS) and Chilean-Pampean flat slabs (27ºS to 33ºS) are tracked beneath the continent for more than 700 km from the trench to the foreland zone (McGeary et al. 1985; Sacks, 1983). In particular, t~~The Chilean-Pampean flat slab has been linked to a broken foreland zone and an eastward expansion of the Neogene to Quaternary arc volcanism that produced an arc gap between 28ºS to 33ºS (Fig. 1) (Allmendinger et al. 1990; Barazangi and Isacks, 1976, 1979; Cahill and Isacks, 1992; Jordan et al. 1983a, 1983b; Kay et al. 1988, 1991; Kay and Abbruzzi, 1996; Pilger, 1981; Ramos et al. 1991, 2002; Smalley and Isacks, 1987; Stauder, 1973; Yañez et al. 2001).

~~Crustal seismicity reflects mountain development over flat subduction settings along the Central Andes (Kay and Coira, 2009; Ramos et al. 2002). In particular,~~ Pardo et al. (2002) refined the shape of the downgoing Nazca Plate from local and teleseismic events beneath the Chilean-Pampean flat slab, showing that at the point of inception of the Juan Fernandez ridge (*JFR*), the plate penetrates to a depth of approximately 100-120 km, with a dip of 30°E, flattening underneath the base of the continental lithosphere for several hundreds of kilometers in coincidence with the Precordillera-Sierras Pampeanas zone (26º-33ºS) (Fig. 1). This slab geometry caused the volcanic arc to migrate as far as 600 km away from the trench (Booker et al. 2004; Martinod et al. 2010). The Juan Fernández ridge at ~32.5ºS coincides with a strong bend of the subducted slab depth contours, at the site of truncation of the active volcanic arc in the models of Barazangi and Isacks (1976, 1979) and Pardo et al. (2002). More recently, this geometry of the southern subducted slab has been refined, showing a more symmetrical geometry around the prolonged eastern edge of the subducted ridge (Anderson et al. 2007), showing the direct relation between the slab flattening and the ridge subduction ~~(Fig. 1).~~

At the northern edge of the Chilean-Pampean flat slab, the Copiapó ridge (Contreras-Reyes and Carrizo, 2011), also known as Easter line (Bonatti et al. 1977) collides with the Chilean trench (Fig. 1 and 2). Even though the potential relation between this feature and the northern shallowing of the Nazca plate at these latitudes has been loosely evaluated in different works (Baker et al. 1987; Bonatti et al. 1977; Comte et al. 2002; González-Ferrán et al. 1985), no geophysical data have been used to determine the track of the Copiapó ridge beneath the South American Plate. We explore in this work the potential role of the Copiapó ridge in the ~~described~~ deformational and volcanic patterns of the overriding plate and the definition of the northern flat slab, through its tracking beneath the continent using gravity data.

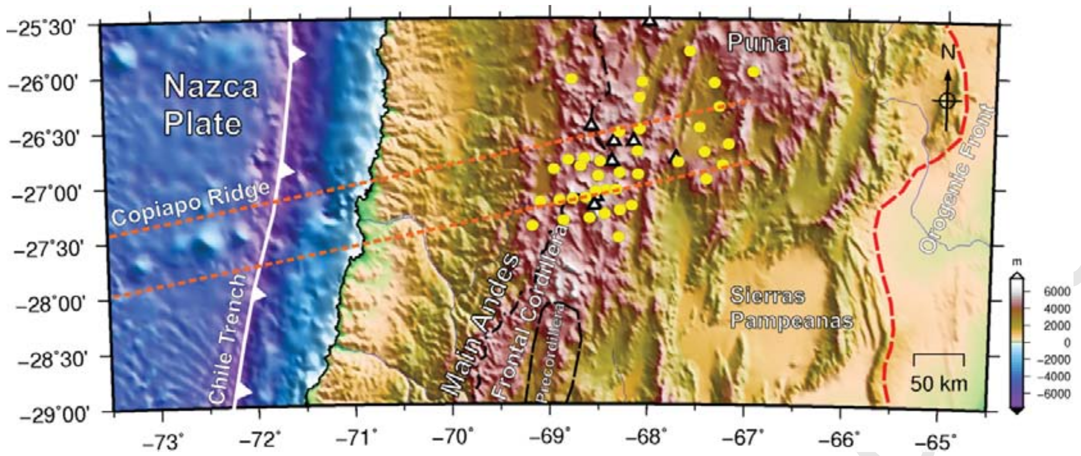

Figure 2. *Shaded digital elevation model at the northern part of de Chilean-Pampean flat slab (see figure 1 for location). White triangles show the southern extent of the active volcanic arc at the transition zone between the 30ºE dipping Nazca plate and the flat slab to the south where a gap in arc activity is established. Red dashed line indicates the eastern orogenic front. Yellow circles depict individual centers of the Ojos del Salado-San Buenaventura volcanic lineament that develop from the arc zone to the retroarc area (Kay et al. 2008; Mpodozis et al. 1996; Seggiaro et al. 2000). Note the general match between the extrapolation of the Copiapó ridge beneath the South American Plate and the Ojos del Salado-San Buenaventura volcanic lineament.*

We calculated the gravity anomaly and vertical gravity gradient for the South Central Andes and adjacent offshore region using the relative high spatial resolution of the global gravity field model EGM2008 (Earth Gravitational Model) and the homogeneous precision of GOCE (Gravity Field and Steady-State Ocean Circulation Explorer) satellite data. Moreover, from the Bouguer anomaly calculated from GOCE data, we computed the crust-mantle discontinuity and the elastic thickness (in the frame of the isostatic lithospheric flexure model applying the method of the convolution approach), with the aim of comparing how these parameters vary in both ridge collisions at the northern and southern ends of the flat slab respectively.

2. GEOLOGICAL SETTING OF THE NORTHERN CHILEAN-PAMPEAN FLAT SLAB (26-28ºS)

At the latitudes of the Chilean-Pampean flat slab (approx. 28ºS to 32ºS) the Andes are formed by a series of mountain systems (Figs. 1 and 2). Namely, from west to east: the Coastal Cordillera, the Frontal Cordillera (which represents the main Andes deformational front), the Precordillera and the Sierras Pampeanas in the foreland. ~~The main Andes project to the north beyond the Chilean-Pampean flat slab into the southern Altiplano region developed at the inner part of the northern Argentinean-Chilean, Bolivia and southern Perú fold and thrust belt (Fig. 2). The main Andes are produced by mechanisms that involve inversion of Late Triassic extensional detachments and subordinately decollement in the Mesozoic and Cenozoic sections (Ramos et al. 1996). The age of these uplifts has been determined as early as late Miocene based on the age of associated synorogenic strata (Jordan and Allmendinger 1986).~~ The Frontal Cordillera and the relief exposed to the east have been related to the inception of the Chilean-Pampean flat slab between 27-33ºS (Ramos et al. 2002). In particular, the Precordillera within this sector is an imbricate system that reactivated Late Triassic detachments and decollements in the Early Paleozoic series, and that together with the Sierras Pampeanas to the east, have been incorporated into the orogenic wedge in the last 10 My (see Ramos et al. 2002, for further references). The Sierras Pampeanas in particular correspond to a classical broken foreland where metamorphosed Paleozoic rocks are exhumed in a Laramide-like way.

These structures have coexisted with an oblique convergence regime between the subducted Nazca and South American plates (Fig. 1) (~ 77ºN respect to the trench) (Angermann et al. 1999; DeMets et al. 1990, 1994, 2010; Kendrick et al. 2003; Ranero et al. 2006; Vigny et al. 2009; Völker et al. 2006). This oblique convergence setting has led to propose a strain partitioned regime favored by the high coupling produced by the flat slab (Chemeda et al. 2000; Gutscher, 1999b, 2000; Pinet and Cobbold, 1992; Pubellier and Cobbold, 1996). In particular, oblique to parallel-to-the-trench regional structures presently act as crustal-scale lateral ramps, partitioning the deformation (Aubry et al. 1996; Baldis and Vaca, 1985; Bassi, 1988; Rossello et al. 1996; Salfity, 1985; Segerstrom and Turner, 1972; Urreiztieta, 1996; Urreiztieta et al. 1996,). Over the Chilean-Pampean flat slab segment, the NNE Calama-Olacapato-El Toro, the Catamarca and the Tucumán lineaments have been associated with strike-slip displacements segmenting the fold and thrust belt (Baldis et al. 1976; Mon, 1976). These structures have also been related to magmatic paths for arc and retroarc volcanism, producing long volcanic alignments in Miocene to Quaternary times (see Kay et al. 2008 and Kay and Coira, 2009 for recent revisions).

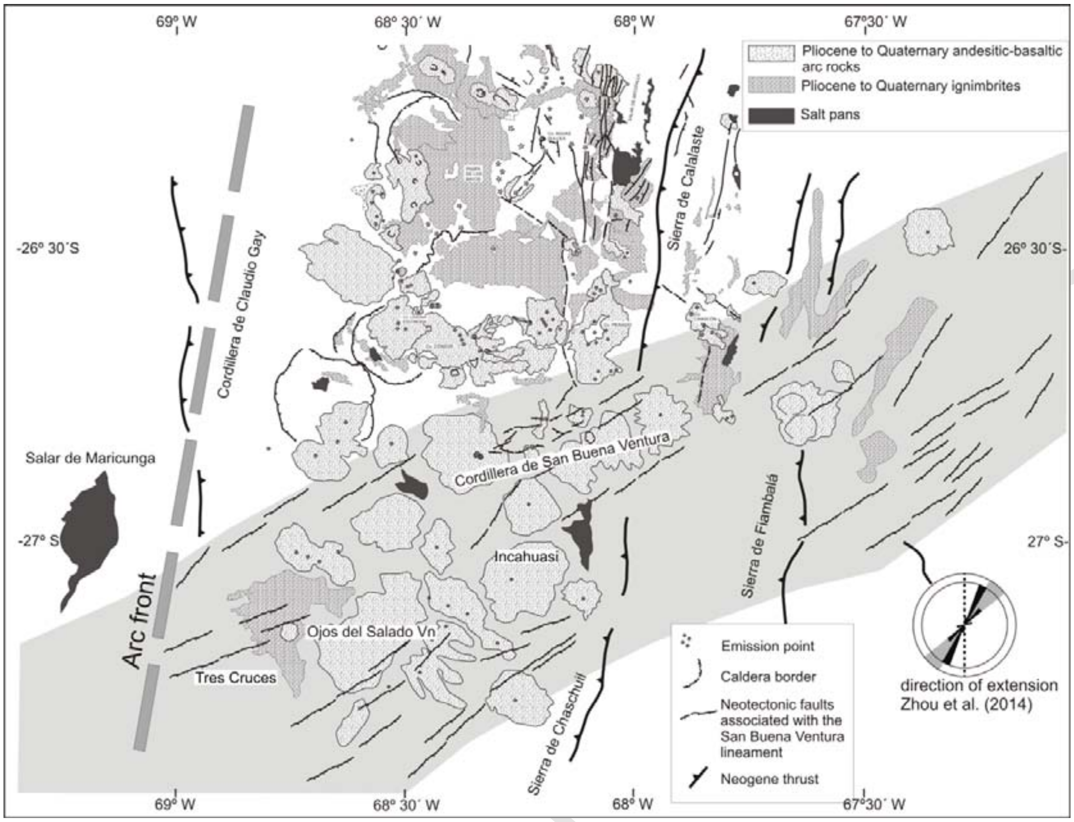

Figure 3. *Pliocene to Quaternary volcanism and related neotectonic structures at the Ojos del Salado-San Buenaventura volcanic lineament shaded in grey (based on Marret et al. 1994; Mpodozis et al. 1996; Seggiaro et al. 2000; Zhou et al. 2014).*

In particular, the ENE-trending Ojos del Salado-San Buenaventura volcanic lineament (Zentilli, 1974) extends at ~27ºS for almost 300 km from the arc front to the retroarc zone (Figs. 2 and 3) (Carter, 1974; Gerth, 1955). This lineament starts at the Chilean Central Valley and crosses the Andes producing a major transverse morphological discontinuity composed of the highest volcanoes of the world such as the Ojos del Salado dome complex and Tres Cruces and Incahuasi stratovolcanoes (Fig. 3) (Bonatti et al. 1977; Mpodozis and Kay, 1992; Mpodozis et al. 1996). This volcanic chain is associated with a strong deflection in the Andean drainage divide from N- in the south to ENE in the north imposed by the aligned summit of stratovolcanoes, calderas and dome complexes (Fig. 2) (Kay et al. 2008). (see Appendix A for a more detailed description) ~~These centers are affected and controlled by normal and right lateral neotectonic structures, defining a general ENE structural alignment (Fig. 3) (Kay et al. 2008; Marrett et al. 1994; Mpodozis et al. 1996; Seggiaro et al. 2000; Zhou et al. 2014). Most of the volcanic centers controlled by these structures are Pleistocene in age, although some show a more prolonged activity during the Holocene (see Appendix A for a more detailed description) (Baker et al. 1987; Kraemer et al. 1999; Montero López, 2009; Mpodozis et al. 1996; Risse et al. 2008; Seggiaro et al. 2000; Viramonte et al. 2008).~~→moved to Appendix A

3. METHODOLOGY: EARTH GRAVITY FIELD MODELS

Satellite only models (e.g. GOCE, Pail et al. 2011) and high-resolution gravity field models based on observations of satellite data plus terrestrial data are available in spherical harmonic expansion (e.g., Earth Gravitational Model 2008, EGM2008 Pavlis et al. 2008). ~~The resolution of the~~ Satellite-only models present ~~is~~ lower resolution than ~~terrestrial data and~~ combined models, although ~~it is~~ they are accurate for interpretation of large-scale structures, especially in high and inaccessible regions such as certain parts of the Andes (Köther et al. 2012). This allows regional gravity modeling, for studies of the lithosphere and crustal anomalies such as regional structures, suture zones, basins and delimitation of magmatic provinces (Álvarez et al. 2012, 2014a,b, 2015; Braitenberg et al. 2011a, 2015; Hirt et al. 2012; Li et al. 2013; Mariani et al. 2013) especially in those regions where terrestrial data are sparse or unavailable due to the limited access. The use of satellite derived models also allows overcoming problems related to non-unified height measurements from different terrestrial campaigns (Gatti et al. 2013; Reguzzoni and Sampietro, 2010). Earth Gravity Field models are presented as sets of coefficients of a spherical harmonic approximation of the gravity field up to a maximum degree N_{max} which governs the spatial resolution of the model (λ) (Barthelmes, 2009; Hofmann-Wellenhof and Moritz, 2006; Li, 2001). EGM2008 is developed up to degree/order 2159 with some additional terms up to degree/order 2190 (Pavlis et al. 2008). The last model derived from data of the satellite GOCE mission (datasheet_go_cons_gcf_2_tim_r4.pdf, http://icgem.gfz-potsdam.de/ICGEM/, Pail et al. 2011) is developed up to a maximum degree and order N=250 (with an effective data volume of approx. 26.5 months). Thus, the spatial resolution for the potential field model EGM2008 becomes equal to $\lambda/2\approx$ 9 km, and $\lambda/2\approx$ 80 km for GOCE.

The gravity field is attenuated at the satellite height, so satellite-only based models achieve a low spatial resolution and provide information only on the long wavelength portion of the spectrum (Reguzzoni and Sampietro, 2010). Despite this disadvantage, GOCE derived models have homogeneous precision, as these have no present sampling errors and biases induced by terrestrial data, as in the EGM2008 model. Statistical results from a comparison analysis between gravity anomalies obtained from both models (Appendix B), up to the same degree/order of the harmonic expansion (N=250), indicate that the fields are only in partial agreement and differences become smooth (Braitenberg et al. 2011a; Alvarez et al. 2012, 2013).

In particular, gravity anomaly and vertical gravity gradient maps obtained from satellite GOCE data in the northern Chilean-Pampean flat slab exhibit a good correlation at medium to high wavelengths with the EGM2008 model, especially over the areas of low topography (Alvarez et al. 2012, 2013). Greater differences between the EGM2008 with respect to the satellite-only model of GOCE arise in the Andean region. North of 28ºS, the high gravimetric effect of the Andean roots masks the crustal structures when using the long wavelength data of GOCE (Alvarez et al. 2012).

Since this work is focused on the evaluation of the interplay between the subduction of an aseismic ridge (Copiapó ridge) and the potential deformational effects in the overriding plate and volcanism along the Ojos del Salado-San Buenaventura volcanic lineament, a gravity data set with a regional coverage without neglecting high frequency data is required. EGM2008 model constitutes a combined solution composed of a worldwide surface gravity anomaly database of 5´x 5´ resolution, and GRACE-derived satellite solutions, that has the advantage of covering both land and marine areas worldwide. Pavlis et al. (2012) indicate that its spectral content was supplemented with gravitational information implied by the topography, only over areas where lower resolution gravity data were available. Over these "fill-in" areas, the gravity anomaly information over the harmonics of degree from 721 to 2159 is supplemented with the gravitational information obtained from the analysis of a global set of Residual Terrain Model-Implied (RTM-Implied) gravity anomalies (i.e. the high frequencies of EGM2008 are calculated from the topography; see Pavlis et al. (2012), for a detailed discussion). The quality and resolution of the downward continued geopotential models in the Andes and Central America decrease with increasing topography and depend on the availability of terrestrial gravity data (Köther et al. 2012). In the study area the 5´x

5′ gravity anomaly (Δg) data sources are NGA-LSC (National Geospatial-Intelligence Agency - Least-Squares Collocation) and some fill-in data in areas covered by proprietary data. The 5′x 5′ Δg data availability shows several lines of available data in our study region (Pavlis et al. 2008). Köther et al. (2012) explained that combined gravity models can be used for density modeling of relatively smaller features such as shallower crustal structures, while satellite-only models are not appropriate for this purpose due to their low spatial resolution. They also mentioned that 3D modeling of synthetic gradients and invariants of subduction zones, using the Andes as case study, proved the applicability of gradient measurements for detection of the edge of geological structures. Therefore, gradients from GOCE mission can resolve structural information (Köther et al. 2012).

Based on the aforementioned, the *Tzz* map of EGM2008 data is preferred to GOCE in order to identify the main structures that affect the upper crust, having a higher spatial resolution. However, in order to calculate different quantities related to a longer wavelength characteristic of the gravity field (Moho and Elastic Thickness) we used the satellite-only model of GOCE which presents homogeneous precision and higher accuracy (see Alvarez et al. 2012, 2014, 2015).

3.1. Gravity anomaly and vertical gravity gradient fields for identifying crustal regional structures

The topography-reduced gravity anomaly (*Ga eq. 1*) (Hofmann-Wellenhof and Moritz, 2006; Molodensky et al. 1945, 1962), a functional of the geopotential (not defined by reduction formulas such as the Bouguer anomaly), is very useful to show the effects of different rock densities within the crust. It is calculated by subtracting the gravity of the reference potential from the observed gravity and then subtracting the effect of the topographic masses above the geoid (see Barthelmes, 2009).

$$Ga = \Delta_{g_{ty}}(h, \lambda, \phi) = g(h, \lambda, \phi) - g_t(h, \lambda, \phi) - \gamma(h - \zeta_g, \phi) \quad (1)$$

Were g is the real gravity, g_t is the effect of the topographical masses above the geoid at a given point (h, λ, ϕ), and γ is the gravity of the reference potential at the same longitude and latitude, but at the ellipsoidal height h-ζ_g (where ζ_g is the generalized height anomaly). The height h is assumed on or outside the Earth surface ($h \geq h_t$).

Gradients of the gravity field highlight main geological features, and allow unveiling unknown structures that are either buried by sediments or just have not been recognized (Braitenberg et al. 2011a). The Marussi Tensor M is composed of five independent elements and is obtained as the second order spatial derivatives of the disturbing potential (Hofmann-Wellenhof and Moritz, 2006). The Marussi tensor components in a spherical coordinate system are given by Tscherning (1976) and by Rummel et al. (2011).

For geological mapping, the second vertical derivative of the disturbing potential (*Tzz* component eq. 2) is ideal, since it highlights the center of the anomalous mass (Braitenberg et al. 2011a). Braitenberg et al. (2011a) explained that even though the Marussi tensor and the gravity field both reflect density variations in the crust, these outline very different subsurface features. In a recent work, Alvarez et al. (2012) showed that both quantities highlight equivalent geological features in a different and complementary way: while *Tzz* highlights mass heterogeneities, where density contrasts are faced, especially in the upper crust, the *Ga* becomes useful when the density contrast is relatively low and the geological structures are deep, where the *Tzz* loses sensitivity (Alvarez et al. 2012).

$$T_{zz} = \frac{\partial^2 T}{\partial r^2} \left[1\,\text{Eötvös} = 10^{-4} \frac{\text{mGal}}{\text{m}} \right] \quad (2)$$

3.1.1. Calculation of *Ga* and *Tzz*

We calculated the vertical gravity gradient and the gravity anomaly (Figs. 4a and b) (Janak and Sprlak, 2006) for the Southern Central Andes, using data of the model EGM2008 up to degree/order N=2159 (Pavlis et al. 2008) on a regular grid with a cell size of 0.05º. The values were calculated in a geocentric spherical coordinate system at a calculation height of 7,000 m to ensure that all values were above the topography.

The topographic effect was removed from the fields to eliminate the correlation with the topography. Topographic mass elements obtained from a global relief model, which includes ocean bathymetry (ETOPO1: Amante and Eakins, 2008), were approximated with spherical prisms of constant density in a spherical coordinate system (Anderson, 1976; Grombein et al. 2010, 2013; Heck and Seitz, 2007; Wild-Pfeiffer, 2008). Spherical prisms are used in order to account the Earth's curvature (Alvarez et al. 2013; Bouman et al. 2013; Uieda et al. 2010). A standard density of 2,670 kg/m^3 was used for masses above sea level and a density of 1,030 kg/m^3 for the sea water. All calculations were carried out with respect to the system WGS84. The topographic correction amounts up to tens of Eötvös for the vertical gradient and up to a few hundreds of mGal for gravity, becoming higher over the maximum topographic elevations (e.g. the Puna and the Main Andes) and lower over the topographic depressions such as the Chilean trench.

3.2. Flexural strength of the lithosphere

The lithospheric strength, related to the thermal state, composition and rheological properties of the crust is well characterized by the flexural rigidity (Lowry et al. 2000). The flexural rigidity (*D*) can be interpreted in terms of the elastic thickness (*Te*) by making assumptions regarding the Poisson ratio (v=0.25) and the Young modulus (E=100GPA=10^{11}N/m^2). Thus, the flexural rigidity can be expressed by:

$$D = T_e^3 . \frac{E}{12(1 - v^2)} \quad (3)$$

The isostatic state and deformation of the upper crust are reflected in the spatial distribution of the *Te*, whose variation can be explained by temperature distribution and a change in the Young modulus. *Te* defines the maximum size and wavelength of the surface loading that can be supported without an elastic break of the lithosphere. Different authors found a correlation between *Te* and the geometry and composition of the flexured plate, external forces and the thermal structure (e.g. Burov and Diament, 1995; Goetze and Evans, 1979; Hackney et al. 2006; Lyon-Caen and Molnar, 1983).

Different methods have been developed, tested and extensively used for estimation of the elastic thickness, as flexural coherence analysis or spectral methods, and recently the convolution approach (Braitenberg et al. 2002, Wienecke 2006, 2007). When calculating the flexural strength of the lithosphere using spectral methods (coherence and admittance) a large spatial window is required over the study area, and the method becomes unstable if the input topography is smooth. Both methods require an averaging process; therefore the variation in rigidity may be retrieved only to a limited extent (Wienecke 2006). For this reason, these techniques have been questioned when applied to continental lithosphere.

The convolution approach is a method of double entry that calculates the flexure parameters by the best fit of the observed crust-mantle interface (e.g. Moho by gravity inversion) and the crust-mantle interface computed due to a flexure model (www.lithoflex.org). This method requires gravity field data on a much smaller scale (on the order of 100 km in length) than when using spectral methods, and allows a relatively high spatial resolution (Braitenberg et al. 2007; Wienecke, 2006). Otherwise, the topography must be known over an extensive scale, which depends on the elastic thickness and therefore the radius of convolution as explained by Wienecke (2006). This method has been extensively tested in synthetic models over different areas worldwide (Alvarez et al. 2014b, 2015; Braitenberg and Drigo, 1997; Braitenberg and Zadro, 1999; Braitenberg et al. 1997; Braitenberg et al. 2002; Bratfisch et al. 2010; Ebbing et al. 2007; Ferraccioli et al. 2011; Steffen et al. 2011; Wienecke, 2002, 2006; Zadro and Braitenberg, 1997). We used Lithoflex software package to accomplish the inverse modeling of *Te* (see Appendix C).

4. RESULTS

4.1. The Copiapó ridge subduction and its deformational effects from EGM2008 derived data

The outer rise east of the Chilean trench produced by the flexure of the downgoing Nazca plate, coincides with a positive *Ga* of about 230 mGal (Fig. 4b), and with a positive *Tzz* anomaly higher than 23 Eötvös (Fig. 4a). Next to it, the Copiapó ridge appears as a well-defined *Tzz* signal higher than 30 Eötvös and a *Ga* higher than 250 mGal. We calculated the path of the Copiapó ridge beneath South America using Euler Poles from Table A1 (Wessel and Kroenke, 1997, 1998; Wessel 1999, 2001, 2008. See table A1 in appendix section) determining its projection in 2 My and 8 My onwards from the point of inception into the trench (Fig. 5a). The backward calculation indicates a probable origin at the Easter (Sala and Gomez) hotspot approximately 40 My ago.

At the latitudes between 26.5º and 27.5ºS, over the South American continent, a rotation in the general strike of the NNE pattern of the *Ga* and *Tzz* anomalies to a general ENE-direction is particularly notorious (Fig. 4a, b). This is interpreted as reflecting a regional rotation in the Andean structures circumscribed to a band coincident with the extrapolation of the Copiapó ridge beneath the South American plate, determined using Euler poles between Nazca and South American plates (Fig. 4 and 5a).

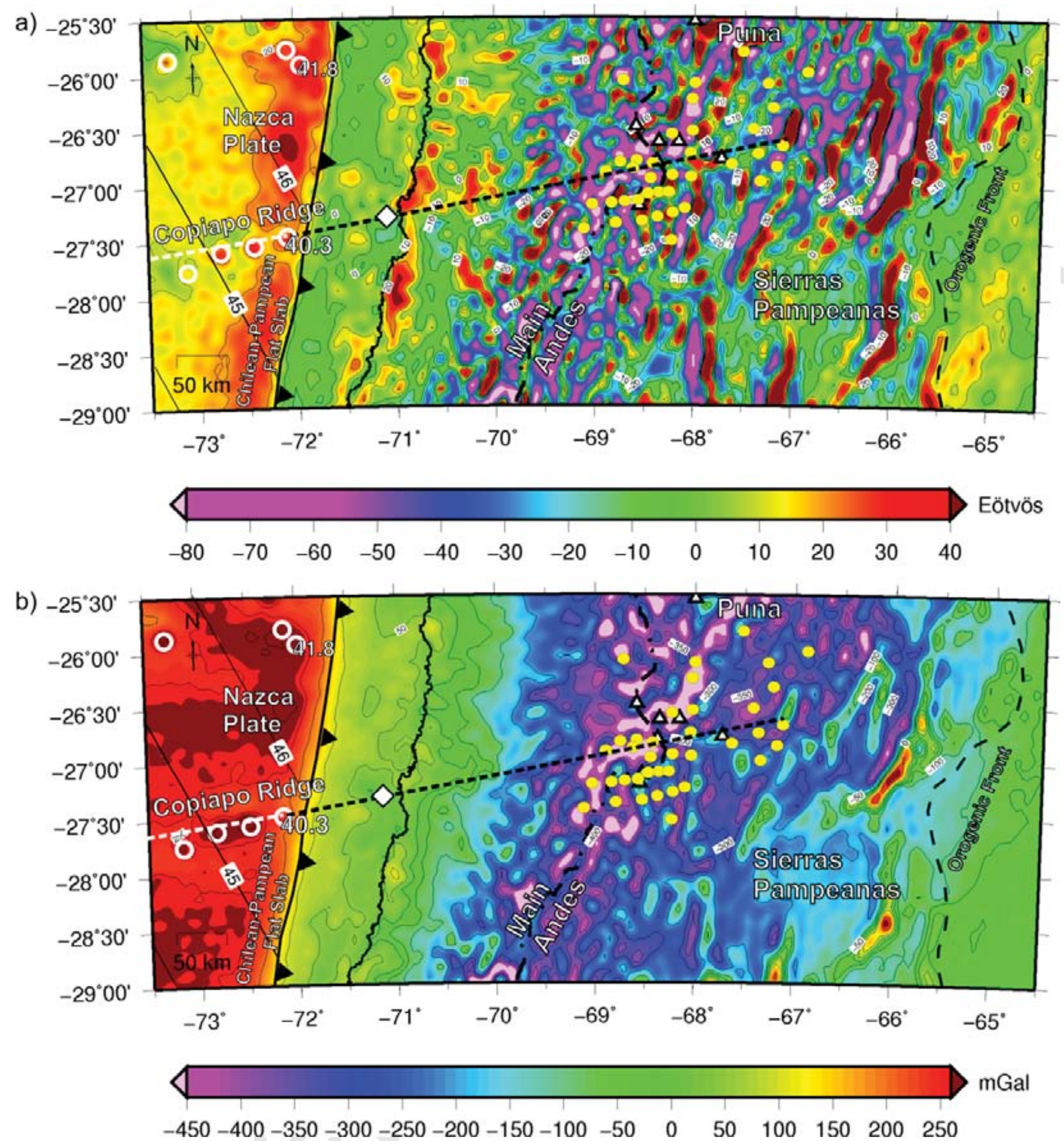

Figure 4. ***a)*** *Vertical Gravity Gradient from EGM2008 corrected by topographic effect in the region of the Copiapó ridge and Ojos del Salado-San Buenaventura volcanic lineament.* ***b)*** *Gravity anomaly computed from ~~the~~ EGM2008 corrected by topographic effect. Superimposed, the computed track of the Copiapó ridge (Fig. 5a) is indicated backward in time (white dashed line) and forward in time (black dashed line). Yellow circles depict individual centers forming the Ojos del Salado-San Buenaventura volcanic lineament (Fig. 2). White circles are seamount locations and age of the*

underlying sea floor in millions of years, from the catalog of Wessel (2001). Solid line indicates oceanic crust ages (Müller et al. 2008). Triangles indicate the current position of the active volcanic arc (Siebert and Simkin, 2002).

The relation between the extrapolation of the Copiapó ridge beneath the South American plate and the change in the general NNE-trend of the Andean structures to an ENE-direction, coincident with the area of the Ojos del Salado-San Buenaventura volcanic lineament, was additionally analyzed by means of the terrain fabric analysis (see Appendix D). Previous works used the eigenvector analysis for detection of lineaments by means of satellite images and digital elevation data (e.g. Koike et al. 1998; Raghavan et al. 1993). In this sense, in a recent work, Beiki and Pedersen (2010) used the eigenvector analysis of gravity gradient tensor to locate geologic bodies.

We used Microdem software to extract the fabric from the vertical gravity gradient, in order to recognize the structural pattern at the site of subduction of the Copiapó ridge (Fig. 5b). We obtained a circular histogram (rose diagram) from the fabric of the *Tzz* for the whole area (black azimuth line in the rose diagram of Fig. 5b) and another for the region (white rectangle in Fig. 5b) where a general deflection of the Andean structures is observed. From the rose diagram, the deflected fabric (to an ENE-direction) along this stripe (grey azimuth line in Fig. 5b) is interpreted as related to a deformational fabric imposed by the subduction of the Copiapó ridge beneath South America.

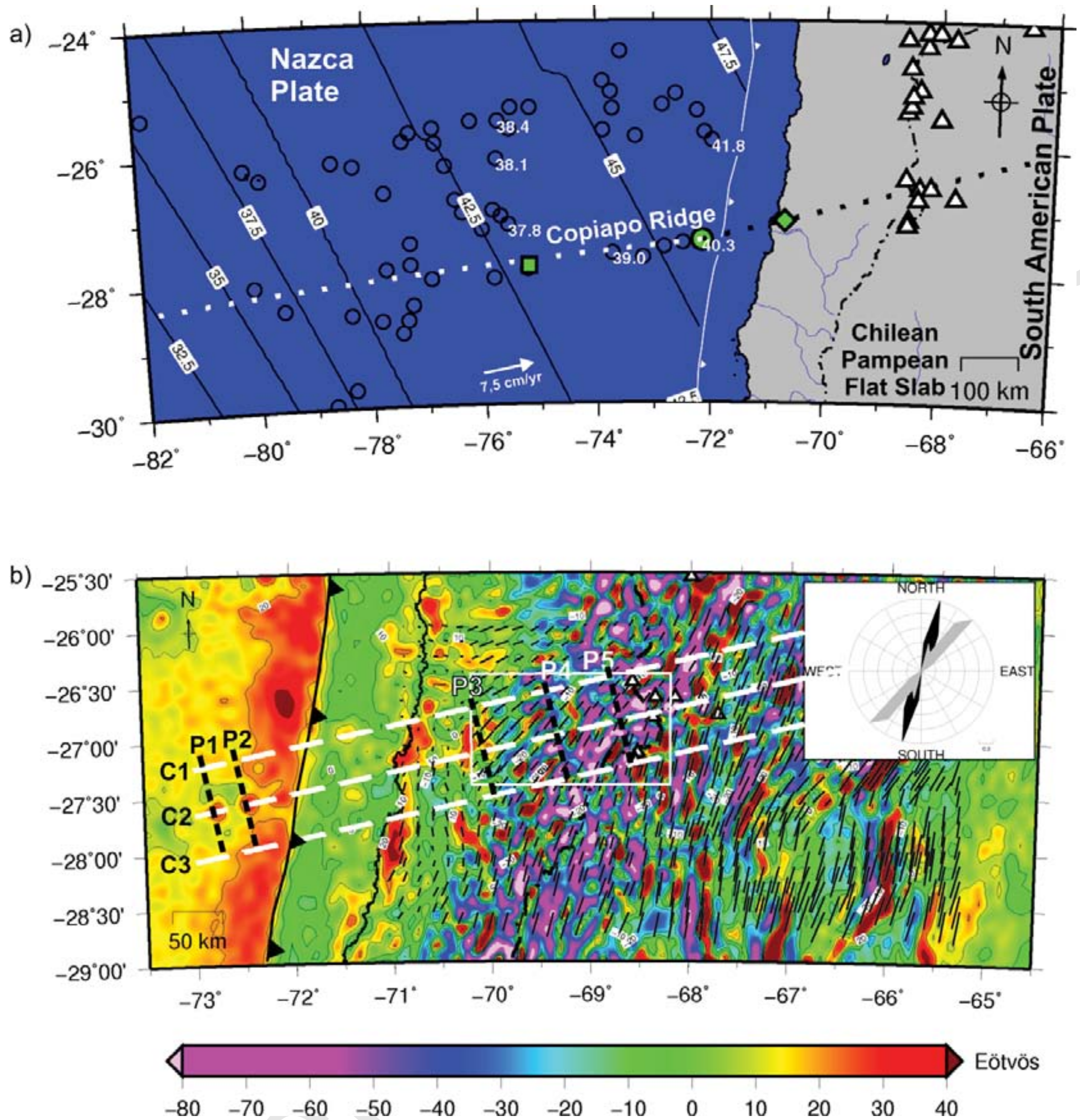

Figure 5. ***a)*** *Reverse and forward reconstruction of the Copiapó ridge trajectories using Müller et al. (2008)´s and DeMets et al. (2010)´s Euler Poles respectively. The green square~~s~~ indicate the corresponding position~~s~~ 2 My ago for ~~two~~ a seamount~~s~~ (green circle) located near the trench, while the green rhomb~~s~~ indicate ~~their~~ it's projected position beneath the continent in 2 My. Triangles indicate the current position of the active volcanic arc (Siebert and Simkin, 2002). Blue circles are seamount locations with the age of the underlying sea floor (My) from the catalog of Wessel (2001). Solid lines indicate oceanic crust ages (Müller et al. 2008).* ***b)*** *Strength*

and orientation of the fabric of the vertical gradient of the gravity field (Tzz), superposed to the vertical gradient of the gravity field at the northern part of the Chilean-Pampean flat slab zone. Note the strong deflection that is observed at the zone of extrapolation of the Copiapó ridge beneath the South American plate. In the upper right corner, a rose diagram shows the deviation from the strikes of the vertical gradient of the gravity field, for the whole study area (black) to the sector where the deflection is inferred to be caused by the Copiapó ridge collision (gray) (white rectangle). White dashed lines are profiles (Ci) of Fig. D1. Black dashed lines are profiles (Pi) of Fig. D2.

4.2. Strength of the lithosphere from GOCE data

The Bouguer anomaly obtained from GOCE data (Fig. 6a) and the gravity anomaly corrected by the topographic effect from EGM2008 (Fig. 4b) show the influence of the Andean roots expressed by regional low gravity values (less than -200 mGal), being lower in the Puna region to the north of the analyzed segment. The positive effect of the Nazca plate is also observed, reaching maximum values at the outer rise area. The Copiapó ridge can be tracked by its well-defined gravity signal, lower than the surrounding oceanic ~~ocean~~ floor (Fig. 6a). Additionally, Moho depths (Fig. 6b) in the oceanic Nazca Plate show the existence of an over thickened crust in coincidence with the ridge path (~15 km). Similarly, the Moho depths increase beneath the *JFR*, as reported by Von Huene et al. (1997) based on wide angle seismic data and by Sandwell and Smith (1997) who related negative satellite derived gravity anomalies to a crustal root indicative of crustal flexure derived from loading.

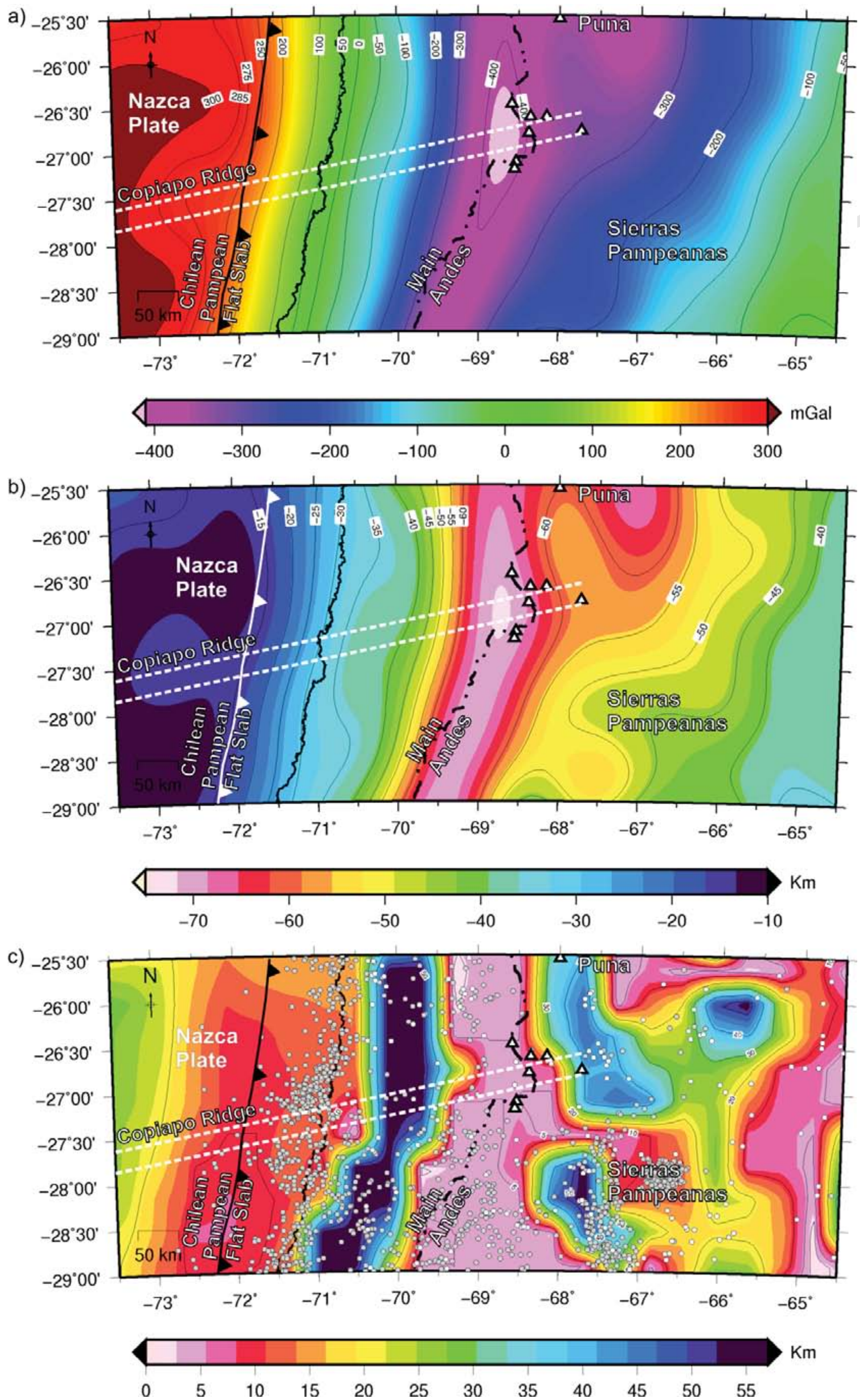

a)
Puna
Nazca Plate
Copiapo Ridge
Chilean Pampean Flat Slab
Main Andes
Sierras Pampeanas
50 km
N
-25°30'
-26°00'
-26°30'
-27°00'
-27°30'
-28°00'
-28°30'
-29°00'
-73°
-72°
-71°
-70°
-69°
-68°
-67°
-66°
-65°
mGal
-400
-300
-200
-100
0
100
200
300
b)
Km
-70
-60
-50
-40
-30
-20
-10
c)
Km
0
5
10
15
20
25
30
35
40
45
50
55

Figure 6. ***a)*** *Bouguer anomaly obtained from GOCE (up to degree/order N=250) corrected for main sedimentary basins. This anomaly has been used to invert the Moho surface. Note an accentuation of the negative anomaly produced by the Andean roots at the site of inception of the Copiapó ridge beneath South America. The Copiapó ridge over the Nazca plate can be discerned by its well-defined gravity signal, lower than the surrounding ocean floor.* ***b)*** *Moho undulations obtained by inversion of the sediment-corrected Bouguer anomaly (GOCE data, Fig. 6a). The obtained Moho depths suggest an over thickened oceanic crust along the ridge path before colliding against the Chilean margin.* ***c)*** *Elastic thickness obtained from GOCE data, superimposed to hypocentral seismicity indicated by small circles (EHB Catalog) (crustal earthquakes are in white and subducted Nazca Plate earthquakes in black) compared to the computed path of the Copiapó ridge. Note a seismic gap onshore along the seamount track that coincides with a site of low Te. Also note how a deepest Moho at the site of interaction between the subducted ridge and the Andean roots is deflected to the east.*

The Bouguer anomaly obtained from GOCE data (Fig. 6a) evidenced a maximum depth of the Andean roots, at the site of inception of the Copiapó ridge beneath South America, reflected in the inverted Moho topography (Fig. 6b). ~~However, a~~ At the forearc region a change in the Moho contours is observed (between -35 to -40 Km) indicating a crust ~~narrowing~~ thickening aligned with the ridge path (Fig. 6b). The same pattern had been reported from seismological data (between -35 to -40 Km) for the *JFR* at the southern part of the Chilean-Pampean flat slab (see Alvarez et al. 2015 and references therein).

Crustal rigidity increases in the forearc over the flat-slab region, as noted in previous works (Alvarez et al. 2014b, 2015; Stewart and Watts, 1997; Tassara, 2005) defining a sharp transition to the south of the Juan Fernandez ridge zone of inception. In particular, elastic thicknesses in the oceanic plate next to the trench (Fig. 7) are higher where the Juan Fernandez ridge intersects the trench. South of *JFR* the forearc exhibits low elastic thicknesses interpreted as the expression of a weakened crust due to the heating of the asthenospheric wedge (Alvarez et al. 2015). A correlation between seismicity (EHB-Catalog) and higher *Te* values exists along the Juan Fernandez ridge path beneath the South American plate (Alvarez et al. 2015). Also, a close correspondence exists between the contours of the subducted Nazca slab (plate morphology) and *Te* variations (higher than 5 km) along the southern region of the flat slab, particularly at the Andes (Alvarez et al. 2014b, 2015).

Contrastingly, the Copiapó ridge path beneath South American presents an aseismic behavior (Fig. 6c). In accordance, *Te* values suggest a lower rigidity than in the interplate zone along the *JFR* path. Despite this, a strong truncation of the 5 km isoline of *Te* along the Copiapó ridge path suggests a higher rigidity respect to its surroundings (Figs. 6c and 7). In order to visualize these changes, we traced three longitudinal cross-sections (see Figure 5b for location) along the path of the Copiapó ridge and to the north and south of it respectively, comparing topography, *Tzz*, Bouguer anomaly and *Te* (see Fig. E1 in Appendix E). We also plotted five 2D profiles across the Copiapó ridge path (see Figure 5b for location) comparing: relief, *Tzz*, Bouguer anomaly, Moho and *Te* (see Fig. E2 in Appendix E).

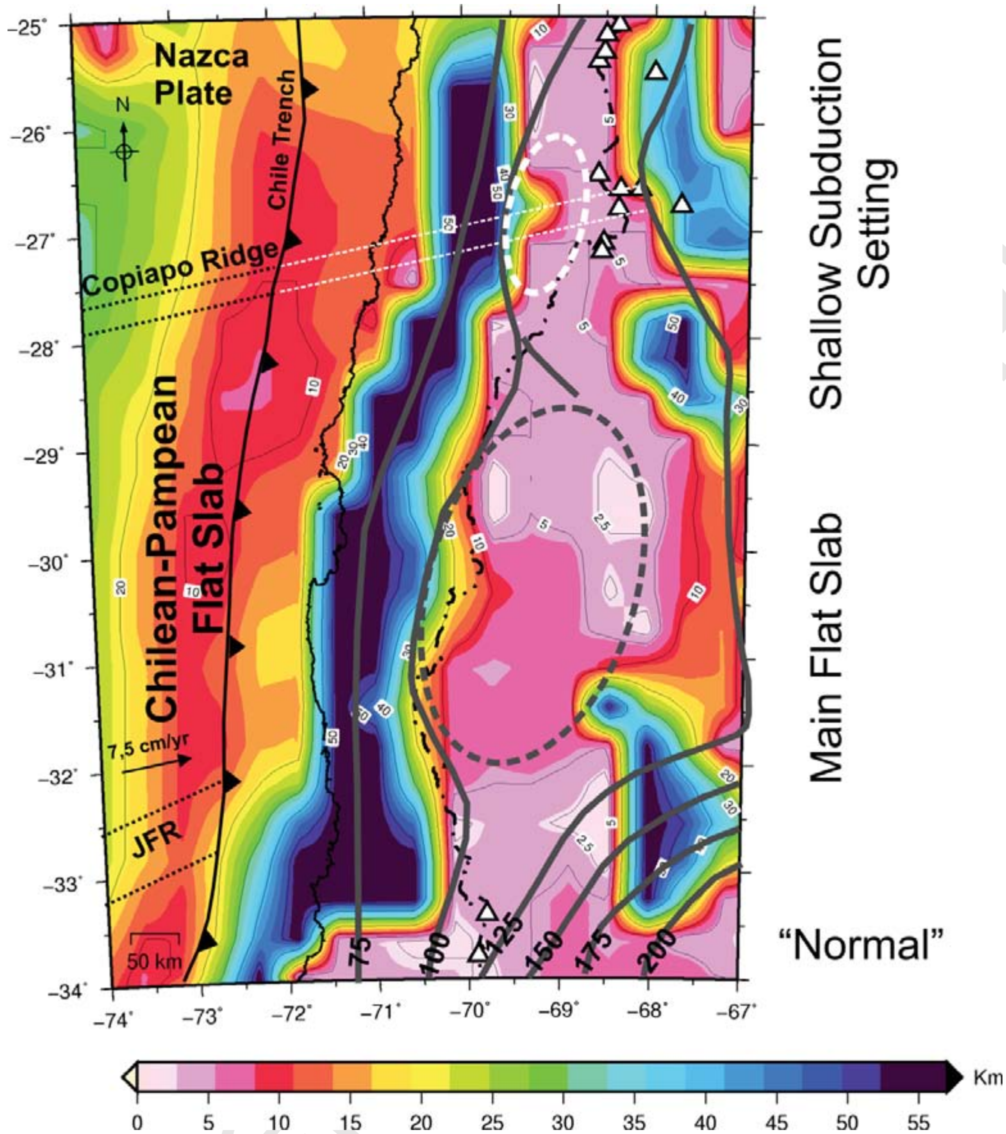

Figure 7. *Elastic thickness obtained from GOCE data. Te presents high values at the forearc in the flat slab region (28.5º to 33ºS) with a higher rigidity at the backarc through the extrapolated path of the JFR. Near the Copiapó ridge, the Te presents a different behavior at the forearc, with high Te values near the trench decreasing eastwards more rapidly than in the JFR region. In spite of this, along the extrapolated path of the Copiapó ridge higher Te values are present, although at a minor scale when compared to JFR. The Wadati-Benioff zone contours (grey solid line) is represented after Mulcahy et al. (2014) (dotted grey ellipse approximates the region where the*

Wadati-Benioff zone is near 100-110 km depth over the Chilean-Pampean flat slab). The dotted white ellipse represents the proposal of a shallow subduction segment potentially related to the subduction of the Copiapó ridge.

4.3. Slab geometry at the site of inception of the Copiapó ridge (26ºS to 28ºS)

Early works had delineated the northern edge of the Chilean-Pampean flat slab across 27-28ºS, as a rather smooth feature, from nearly flat in the south to “normal” in the north (~30ºE) (Araujo and Suarez, 1994; Bevis and Isacks, 1984; Cahill and Isacks, 1992; Jordan et al. 1983a; Pardo et al. 2002; Smalley and Isacks, 1987). More recently new seismic experiments have allowed defining more clearly a sharper transition (Fig. 8b) between these segments (Mulcahy et al. 2014).

We projected hypocenters within the latitude window of 27.5ºS using the CMT locations and EHB-Catalog. Figures 8a and 9a show that the plate subducts sub-horizontally for the first 200 km, and then penetrates into the asthenosphere with an approximate angle of 20ºE. The catalog of focal mechanisms determined by the Harvard Centroid Moment Tensor catalog (Harvard CMT, Global CMT Project, 2006) is obtained by means of the centroid moment tensor method (CMT). This consists in the inversion of two parts of the seismogram, 1) body waves of long period and 2) surface waves of very long period (Stein and Wysession, 2003). CMT solutions use complete waveforms, resulting in the centroid, or average location, in space and time, of the released seismic energy, so depth data can be considered reliable. Additionally, the EHB-Catalog (EHB-Catalog, 2009; Engdahl et al. 1998) has a more reliable location of earthquakes in the study region (Fig. 8a).

In map view (Fig. 8a), the 160 km iso-depth contour clearly depicts the shallow to flat-slab geometry getting a more symmetrical shape in map view than in the initial proposals of Cahill and Isacks (1992). Recent seismic surveys (Mulcahy et al. 2014) using local networks confirm this morphology with a steep edge of the flat slab near 27ºS (Figs. 8b and 9b).

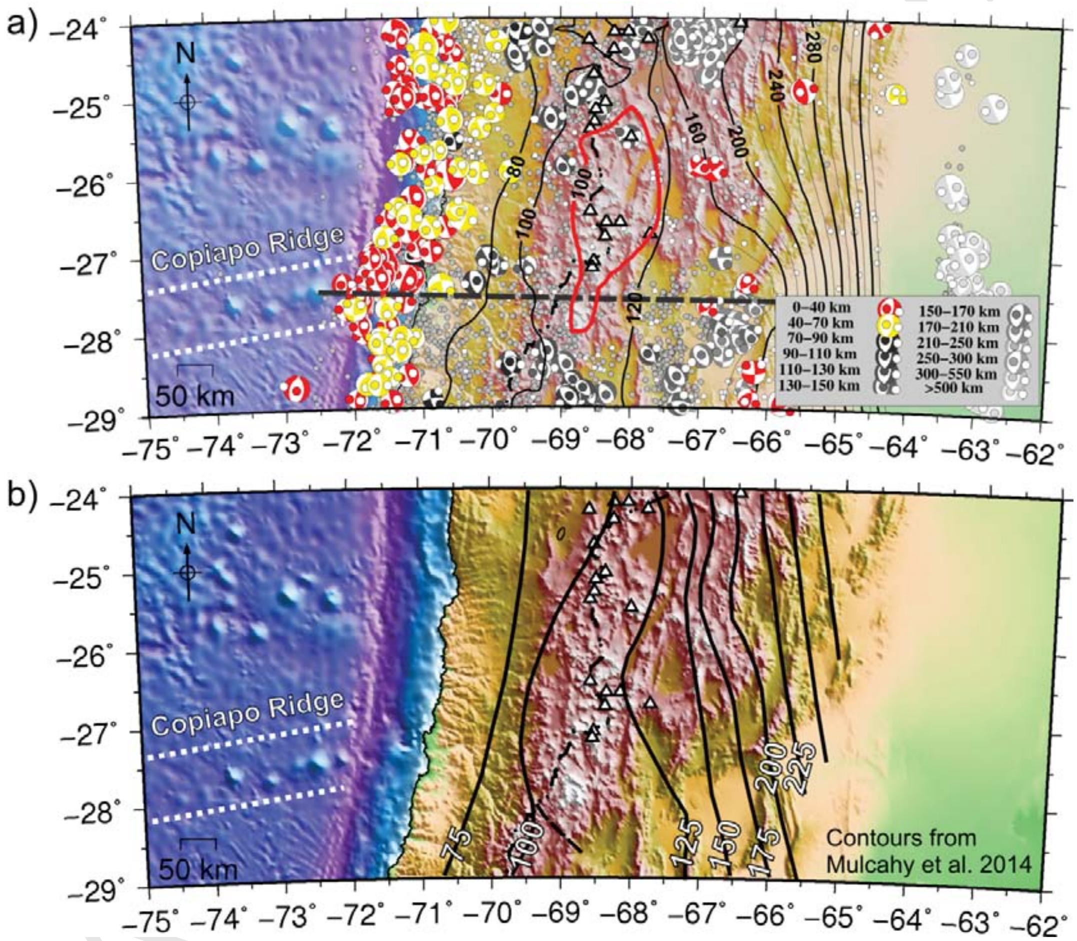

Figure 8. a) *Iso-depth contours and focal mechanisms associated with the downgoing Nazca plate in the northern region of the Chilean-Pampean flat slab and active crustal structures of the Andes. The 160 km iso-depth contour depicts clearly the Chilean-Pampean flat-slab geometry. The shallowing of the subducted Nazca Plate observed at the inception point of the Copiapó ridge is highlighted as a red contour. Hypocentral*

seismicity is indicated with small circles (EHB Catalog) (crustal earthquakes are in white and subducted Nazca Plate earthquakes in black). Focal Mechanisms are from CMT Harvard Catalog. Black dashed line indicates cross section in Figure 9. ***B)*** *Contoured depths of the Wadati-Benioff Zone from Mulachy et al. (2014) at 25 km intervals, shown in black. Both contour families (a and b) show a shallower subducted Nazca Plate at the inception point of the Copiapó ridge.*

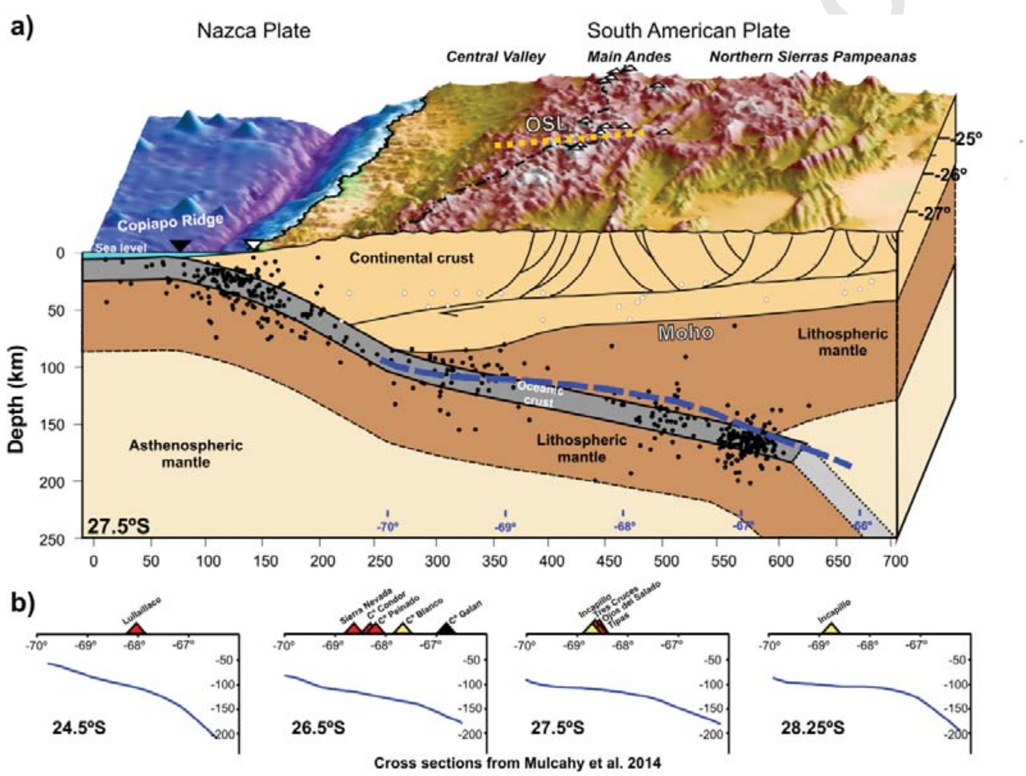

Figure 9a. *Digital elevation model in perspective with crustal cross section at 27.5°S based on Salfity et al. (2005) (azimuth 92.5°; +/- 50 km wide; 0-650 km depth). Interpreted Wadati-Benioff zone at these latitudes is determined by hypocentral seismicity indicated with black circles (EHB Catalog). Crustal earthquakes are indicated as small white circles. As a reference, a cross section at 27.5ºS from Mulcahy et al. (2014) is shown (blue dashed line). Crust-mantle boundary (Moho) is determined*

from the Bouguer anomaly field applying gravity inverse calculations using Lithoflex software package (www.lithoflex.org, Braitenberg et al. 2007; Wienecke et al. 2007). Individual centers at the active arc front are indicated with white triangles (from Siebert and Simkin, 2002). OSL is the Ojos del Salado-San Buenaventura volcanic lineament. Chilean trench and coastline are indicated by black and white triangles respectively. ***b.*** *Series of east-west cross sections representing the Wadati-Benioff zone (indicated in blue) from Mulcahy et al. (2014) showing how the flat slab is well developed south of 28.25ºS, while at 27ºS indicates a shallow subduction setting.*

5. DISCUSSION AND CONCLUDING REMARKS

Flat subduction settings modify the pattern of seismicity, volcanism and deformation in the overriding plate. Results from analogue modeling (Martinod et al. 2013) show that indentation of an overriding plate during ridge subduction is usually accommodated by a complex pattern of structures that include trench-perpendicular strike-slip faults. In particular, the Ojos del Salado-San Buenaventura volcanic lineament represents an anomaly in the pattern of arc-retroarc volcanism at the northern extreme of the Chilean-Pampean flat slab (Figs. 2, 3, A1 and A2). These volcanic centers are controlled by ENE-oriented regional neotectonic structures with dip and strike-slip strain components that project into the retroarc zone transversally to the arc front. ~~Results from analogue modeling (Martinod et al. 2013) show that indentation of the overriding plate during ridge subduction is usually accommodated by trench-perpendicular strike-slip faults.~~ Locally, this volcanic lineament coincides with a strong deflection in the fabric of the Andean deformation visualized from the gravity analyses (Fig. 5b). The observed rotation in the general strike of the NNE "Andean" pattern (Fig. 4a, b) of the *Ga* and *Tzz* anomalies (obtained from EGM2008 model) is consistent with a strong deflection in the Andean drainage divide to ENE in this region; imposed by the aligned summit of volcanic centers and neotectonic structures associated with the Ojos del Salado-San Buenaventura volcanic chain. More specifically the volcanic centers (yellow circles of Fig. 4a) coincide with positive values of the *Tzz* signal (relatively denser bodies are related to a positive *Tzz*) and with relatively higher values in the *Ga*, indicating higher density materials (or a positive density contrast).

These anomalous neotectonic pattern and volcanic alignment across the Andes at about 27.5ºS could be spatially linked to the collision of the Copiapó aseismic ridge. The strike ~~Direction~~ of the Copiapó ridge parallels the plate convergence direction between the Nazca and South American plates (78.1º azimuth NE in our study area, Kendrick et al. 2003), determining a stationary collisional point (Fig. 5b), similarly to the point of inception of the Juan Fernández ridge to the south in the last 10 My (Yáñez et al. 2001). Therefore, the deformational imprint over the upper plate would be expected to have affected a discrete area ~~zone~~, producing an ENE-localized deformational zone, explaining the local deflection of gravity anomalies (Fig. 11). Similarly, neotectonic deformation acquires, east of the arc front, a predominant E-NE orientation along the San Buenaventura volcanic alignment (Seggiaro et al. 2000; Zhou et al. 2014). This deformation is clearly depicted by the *Tzz* (from EGM2008 model) that constitutes a gravity derivative that highlights superficial density anomalies. Thus, it allows the detection of the edge of geological structures and to distinguish the signal due to a smaller shallow density variation from an extensive deeper mass. The spectral power of *Tzz* signal is pushed to higher frequencies, resulting in a signal more focalized to the source than the *Ga* (Li 2001), being the last more sensitive to regional signals and deeper sources (Alvarez et al. 2012). The long wavelength signal from GOCE model also shows an eastward deflected *Ga,* suggesting that the upper crust deformation showed by the *Tzz* could be related to deeper sources; connected by oblique-to-the-Andes intracrustal structures acting as magmatic paths for arc and retroarc volcanism, promoting long volcanic alignments as the OSL-San Buenaventura.

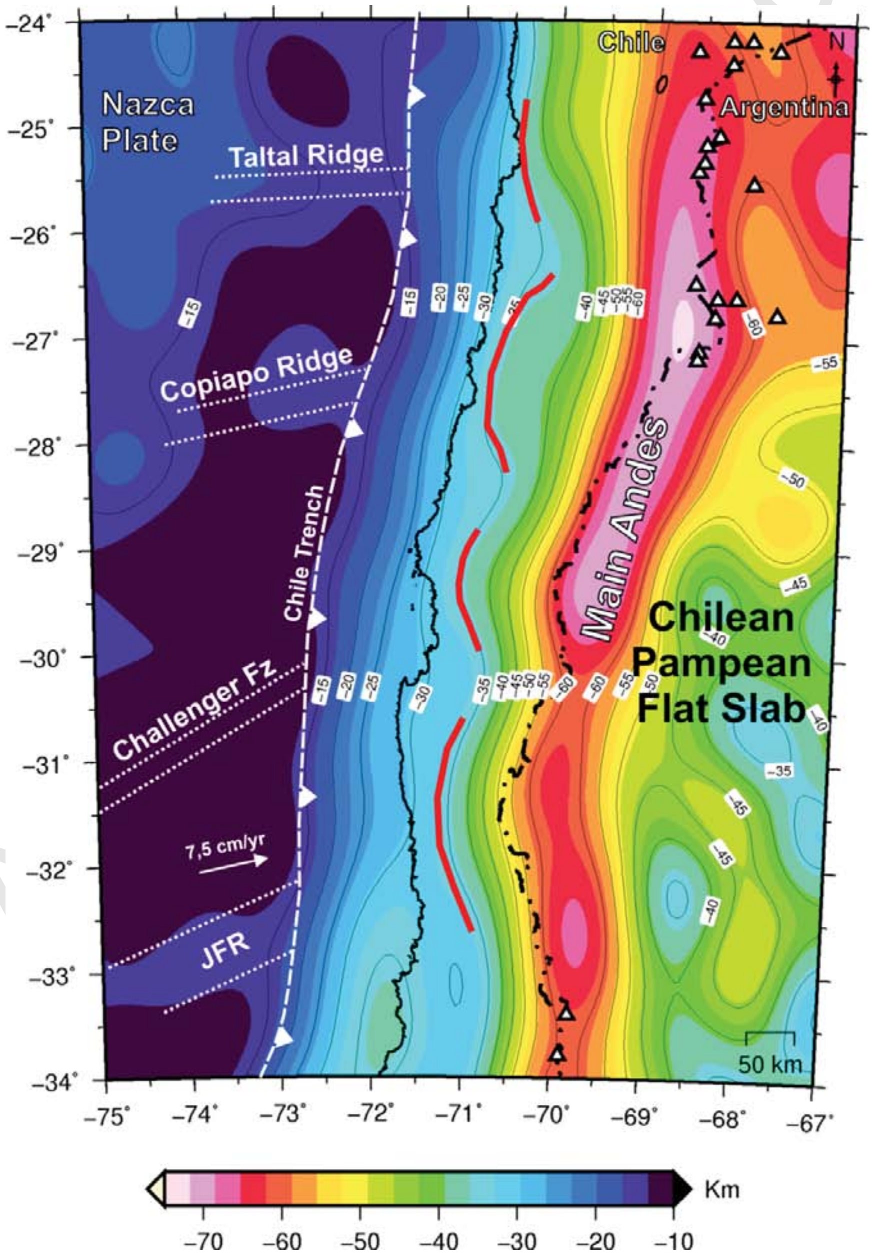

Figure 10. *Moho depth determined from inversion of GOCE data between 25ºS and 34ºS. Note from the forearc to the arc regions an anomalous Moho thickening at the sites of inception of four high oceanic features (anomalous buoyant oceanic crust)* ~~*aseismic ridges*~~ *in the Chilean-Peruvian trench, and in particular at the sites of inception of the Juan Fernández and Copiapó ridges.*

~~A maximum crustal thickness at the arc zone is inferred at the zone of inception of the Copiapó ridge from inversion of gravity data (Fig. 6b). Similarly, at the forearc region a relative crustal thickening respect to neighbor segments is inferred from inversion of gravity data (Fig. 6b).~~ From inversion of gravity data, we obtained a maximum crustal thickness at the arc and forearc zones, coincident with the path of subduction of the Copiapó ridge (Fig. 6b). In fact, crustal thickening at the forearc ~~zone~~ can be checked in this model throughout each zone of inception of a high oceanic feature that impact against the Chilean subduction margin such as the *JFR*, Challenger Fz, Copiapó and Taltal ridges (Fig. 10). ~~Lower crustal thickening~~ Crustal thickening at the forearc and arc zones, as well as extensional and strike slip deformation affecting the upper crust and ~~related~~ controlling volcanism at the Ojos del Salado-San Buenaventura volcanic lineament could be interpreted as a consequence of higher coupling, localized shortening, underplated volcanic materials and regional upward doming. Upper crustal uplift is evidenced by high positive *Tzz-EGM2008* values over the volcanic centers, while the thickening of the lower crust is detected by negative *Ga-GOCE* at the site of ridge subduction over the flat slab zone.

On a more general perspective, flat to shallow subduction zones around the world can be separated in two general groups based on their size. Small zones such as the one associated with the collision of the Carnegie ridge in Ecuador and the one related to the subduction of the Juan de Fuca plate next to Vancouver island in Canada, and large flat slabs such as the Peruvian and the Chilean-Pampean along the central South American subduction margin (Gutscher et al. 2000). In particular the Peruvian and the Chilean-Pampean flat slabs at both sides of the Altiplano-Puna plateau are the most important in terms of size and associated crustal deformation. Particularly, the Peruvian flat slab has been related to the collision of two aseismic ridges, one completely subducted beneath the South American plate (Gutscher 1999a; Rosenbaum et al. 2003; Rousse et al. 2003). Contrastingly, the Chilean-Pampean flat slab has been assigned to the collision of a single aseismic ridge, explaining the extent of this zone by a broken geometry of the subducted ridge beneath the South American plate (Anderson et al. 2007; Yañez et al. 2001).

The Benioff zone geometry at the northern region of the Chilean-Pampean flat slab (Fig. 7) presents a strong change in the slab dip from normal to shallow. Recent works based on local seismic networks (Mulcahy et al. 2014) show that the northern and southern terminations of the flat slab are more abrupt than previously determined, resulting in a flat slab configuration rather symmetrical in map view. Additionally, both edges of the flat slab coincide with the sites of inception of the Copiapó and Juan Fernandez ridges respectively. In this sense, the development of the Chilean-Pampean flat slab could be a function of two simultaneous ridge collisions, similarly to the Peruvian flat slab to the north (Figs. 11 and 12). Finally, this study exemplifies how the Earth Gravity Model EGM2008, used in combination with the newest satellite GOCE data, can be used to track the fate of certain subducted bathymetric anomalies beneath the upper plate of a subduction zone, connecting anomalously thickened ~~subducted~~ oceanic crust, deformational effects, *Te* anomalies, seismic patterns and variable crustal thickness in the overriding plate~~, and variable crustal thickness.~~

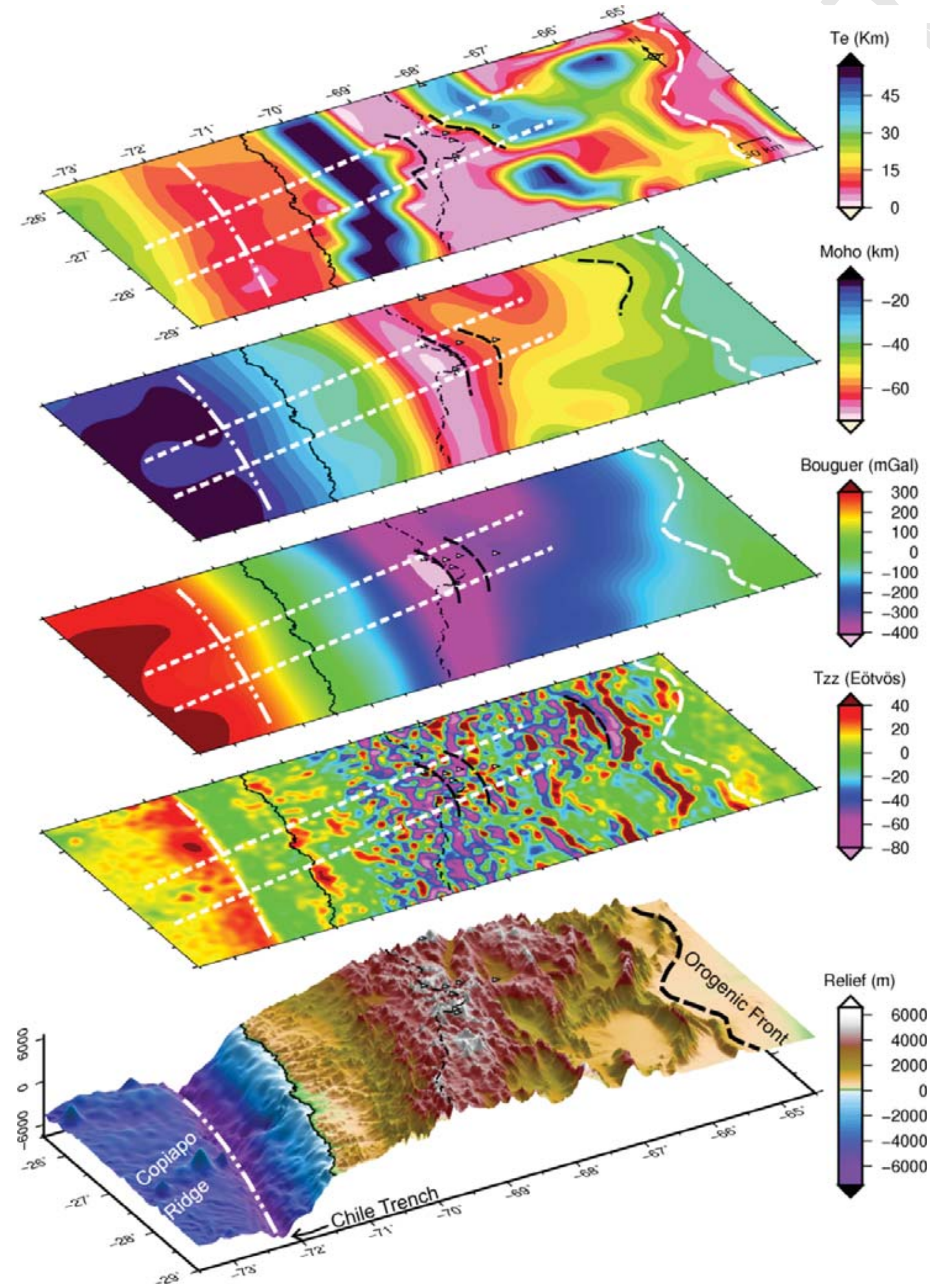

Figure 11. *Relation between the elastic thickness, Moho, Bouguer anomaly, Tzz and topography at the area of inception of the Copiapó ridge beneath the South American plate. Note the relation between the extrapolated ridge path and the change in orientation and truncation of the anomalies highlighted in the gradient signal (Tzz), the eastward deflection observed in Bouguer anomaly, a deeper Moho topography and higher Te values.*

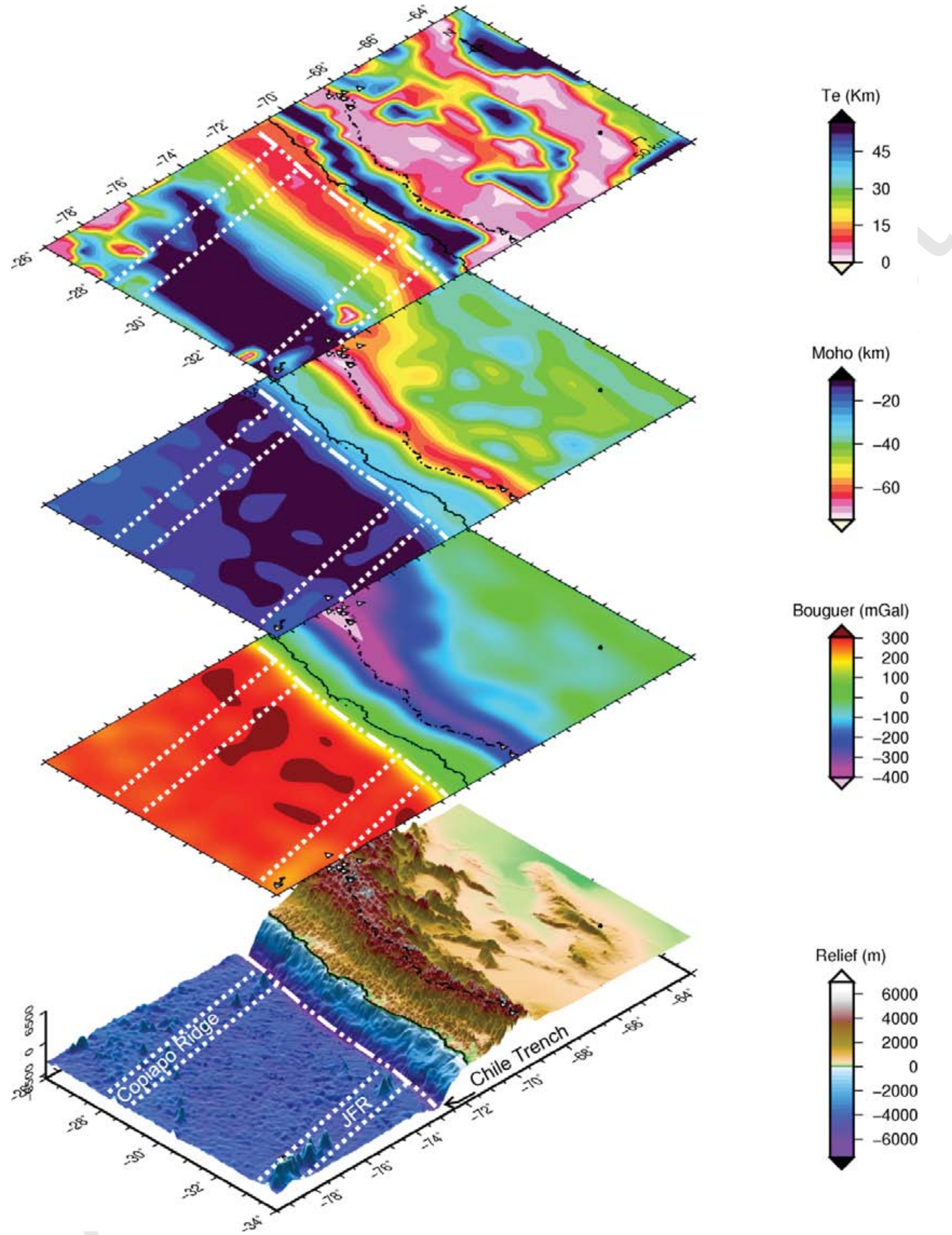

Figure 12. *Two ridge collisions and crustal structure at the Chilean-Pampean flat slab. Note similar rigidity structure and Moho amplitudes at both sites of ridge inception. While the southern ridge collision (Juan Fernández ridge) is linked to a flat slab configuration without arc magmatism, the northern collision coincides with a shallow*

subduction configuration that passes transitionally to a normal subduction setting in the north, with a volcanic arc migrating eastwards at the site of inception of the Copiapó ridge beneath the South American continent.

ACKNOWLEDGMENTS: Authors acknowledge the use of the GMT-mapping software of Wessel and Smith (1998). We greatly acknowledge S.M. Kay for discussion. The authors would like to thank the Ministerio de Ciencia y Técnica – Agencia de Promoción Científica y Tecnológica, PICT07–1903, Agenzia Spaziale Italiana for the GOCE-Italy Project, the Ministero dell'Istruzione, dell'Universita' e della Ricerca (MIUR) under project PRIN, 2008CR4455_003 for financial support, and ESA for granting of AO_GOCE_proposal_4323_Braitenberg.

REFERENCES

Allmendinger, R.W., Figueroa, D., Snyder, D., Beer, J., Mpodozis, C., Isacks, B.L., 1990. Foreland shortening and crustal balancing in the Andes at 30ºS Latitude. Tectonics, 9: 789-809.

Alvarez, O., Gimenez, M., Braitenberg, C., Folguera, A., 2012. GOCE satellite derived gravity and gravity gradient corrected for topographic effect in the South Central Andes region. Geophysical Journal International, 90(2): 941–959, doi: 10.1111/j.1365-246X.2012.05556.x

Alvarez O., Gimenez, M.E., Braitenberg, C., 2013. Nueva metodología para el cálculo del efecto topográfico para la corrección de datos satelitales. Revista de la Asociación Geológica Argentina, 70 (4): 422-429.

Álvarez, O., Nacif, S., Gimenez, M., Folguera, A., Braitenberg, A., 2014a. Goce derived vertical gravity gradient delineates great earthquake rupture zones along the Chilean margin. Tectonophysics, 622: 198-215. http://dx.doi.org/10.1016/j.tecto.2014.03.011

Álvarez O., Giménez M., Folguera A., Spagnotto S., Braitenberg, C., 2014b. El ridge Copiapó y su relación con la cadena volcánica ojos del salado-buena ventura, y con la zona de subducción plana pampeana. Actas del XIX Congreso Geológico Argentino, Córdoba 2014, Simposio S20: Subducción horizontal en el segmento andino 27º-33ºS: Un enfoque multidisciplinario.

Alvarez, O., Gimenez, M.E., Martinez, M.P., LinceKlinger, F., Braitenberg, C., 2015. New insights into the Andean crustal structure between 32° and 34°S from GOCE satellite gravity data and EGM2008 model. In: Sepúlveda SA, Giambiagi LB, Moreiras SM, Pinto L, Tunik M, Hoke GD, Farías M (Eds.), 2015. Geodynamic Processes in the Andes of Central Chile and Argentina, Geol Soc Lond Spec Pub 399, 183–202 (http://dx.doi.org/10.1144/SP399.3). First published online February 6, 2014.

Amante, C., Eakins, B.W., 2008. ETOPO1 1 Arc-Minute Global Relief Model: Procedures, Data Sources and Analysis, National Geophysical Data Center, NESDIS, NOAA, U.S. Department of Commerce, Boulder, CO.

Anderson, E.G., 1976. The effect of topography on solutions of Stokes' problem, Unisurv S-14, Rep, School of Surveying, University of New South Wales, Kensington.

Anderson, M.L., Alvarado, P., Beck, S., Zandt, G., 2007. Geometry and brittle deformation of the subducting Nazca plate, central Chile and Argentina. Geophysical Journal International, 171(1): 419-434, doi:10.1111/j.1365-246X.2007.03483.x.

Angermann, D., Klotz, J., Reigber, C., 1999. Space-geodetic estimation of the Nazca-South America Euler Vector. Earth and Planetary Science Letters, 171: 329-334.

Araujo, M., and Suarez, G., 1994. Geometry and state of stress of the subducted Nazca plate beneath central Chile and Argentina: evidence from teleseismic data. Geophysical Journal International, 116: 283-303.

Arnosio, M., Becchio, R., Viramonte, J.G., de Silva, S., Viramonte, J.M., 2008. Geocronología e isotopía del Complejo Volcánico Cerro Blanco: un sistema de calderas cuaternario (73-12 ka) en los Andes Centrales del sur. Actas 17° Congreso Geológico Argentino, 1: 177-178, Jujuy.

Aubry, L., Roperch, P., Urreiztieta, M., Rossello, E., and Chauvin, A., 1996. A paleomagmetic study along the south-eastern edge of the Altiplano-Puna: Neogene tectonic rotations. Journal of Geophysical Research, v. 101, no. B8, p. 17883-17899.

Baker, P.E., González Ferrán, O., and Rex, D.C., 1987, Geology and geochemistry of the Ojos del Salado volcanic region, Chile. Journal of the Geological Society of London, 144: 85-96.

Baldis, B.A., Vaca, A., 1985. Megafracturas relacionadas con el sistema cordillerano, in Proceedings, 1th Jornadas sobre Geología de la Precordillera, San Juan, Argentina, Actas I, p. 204-208.

Baldis, B.A., Gorroño, A., Plozkiewcs, J., Sarudiansky, R., 1976. Geotectónica de la Cordillera Oriental, Sierras Subandinas y comarcas adyacentes, in Proceedings, 6th Congreso Geológico Argentino, Buenos Aires, Argentina, Actas I, p. 3-22.

Barazangi, M., Isacks, B., 1976. Spatial distribution of earthquakes and subduction of the Nazca Plate beneath South American. Geology, 4: 686-692.

Barazangi, M., and Isacks, B., 1979. Subduction of the Nazca plate beneath Peru evidence from spatial distribution of earthquakes. Geophysical Journal of the Royal Astronomical Society, 57: 537-555.

Barredo, S., Cristallini, E., Zambrano, O., Pando, G., García, R., 2008. In Proceedings, VII Congreso de Exploración y Desarrollo de Hidrocarburos, Noviembre 2008, Actas, p. 443-446. ISBN 978-987-9139-51-6.

Barthelmes, F. 2009. Definition of functionals of the geopotential and their calculation from spherical harmonic models, Theory and formulas used by the calculation service of the International Centre for Global Earth Models (ICGEM), Scientific Technical Report STR09/02, GFZ German Research Centre for Geosciences, Postdam, Germany, http://icgem.gfz-postdam.de

Bassi, H.L., 1988. Hypotesis concearning a remagenic network controlling megtallogenic and other geologic events in the South American Austral Cone. Geologisches Rundschau, 77(2): 491-511.

Beiki, M., Pedersen, L.B., 2010. Eigenvector analysis of gravity gradient tensor to locate geologic bodies. Geophysics, 75(5): 137-149, doi: 10.1190/1.3484098

Bevis, M., Isacks, B.L., 1984. Hypocentral trend surface analysis: probing the geometry of the Benioff zone. Journal of Geophysical Research, 89: 6153-6170.

Bonatti, E., Harrison, C.G.A., Fisher, D.E., Honnorez, J., Schilling, J.G., Stipp, J.J., Zentilli, M., 1977, Easter volcanic chain (southeast Pacific): a mantle hot line. Journal of Geophysical Research, 82(17): 2457-2478.

Bomfim, E.P., Braitenberg, C., Molina, E.C. 2013. Mutual Evaluation of Global Gravity Models (EGM2008 and GOCE) and Terrestrial data in Amazon Basin, Brazil. Geophysical Journal International, 195, 2, 870-882. doi: 10.1093/gji/ggt283

Booker, J.R., Favetto, A., Pomposiello, M.C., 2004. Low electrical resistivity associated with plunging of the Nazca flat slab beneath Argentina. Nature, 429: 399-403.

Bouman, J., Ebbing, J., Fuchs, M., 2013. Reference frame transformation of satellite gravity gradients and topographic mass reduction. Journal of Geophysical Research, Solid Earth, 118(2): 759-774. DOI: 10.1029/2012JB009747

Braitenberg, C., 2015. Exploration of tectonic structures with GOCE in Africa and across-continents. International Journal of Applied Earth Observation and Geoinformation, 35, 88–95.

Braitenberg, C., Drigo, R., 1997. A crustal model from gravity inversion in Karakorum: in Proceedings, International Symposium on current crustal movement and hazard reduction in East Asia and South-East Asia, Wuhan, November 4-7, p. 325-341.

Braitenberg, C., Zadro, M., 1999. Iterative 3D gravity inversion with integration of seismology data: Bollettino di Geophisica Teorica ed Applicata, in: Proceedings, 2º Joint Meeting IAG, Trieste, v. 40, no. 2.

Braitenberg, C., Pettenati, F., Zadro, M., 1997. Spectral and classical methods in the evaluation of Moho undulations from gravity data: the NE Italian Alps and isostasy. Journal of Geodynamics, 23:. 5-22.

Braitenberg, C., Ebbing, J., Götze, H.J., 2002. Inverse modelling of elastic thickness by convolution method-the Eastern Alps as a case example. Earth Planetary Science Letters, 202: 387-404.

Braitenberg, C., Wienecke, S., Ebbing, J., Bom, W., Redfield, T., 2007. Joint gravity and isostatic analysis for basement studies-a novel tool, in Proceedings, EGM 2007 International Wokshop, Innovation on in EM, Grav. and Mag. Methods: a new perspective for exploration, Villa Orlandi Capri, Extended Abstracts.

Braitenberg, C., Mariani, P., Ebbing, J., . Sprlak, M., 2011a. The enigmatic Chad lineament revisited with global gravity and gravity-gradient fields, in Van Hinsbergen, D.J.J., Buiter, S.J.H., Torsvik, T.H., Gaina, C., and Webb, S.J., eds., The Formation and Evolution of Africa: A Synopsis of 3.8 Ga of Earth History: Geological Society of London Special Publication, London, 357: 329–341, doi:10.1144/SP357.18.

Braitenberg, C., Mariani, P., Pivetta, T., 2011b. GOCE observations in exploration geophysics, in Proceedings, 4th International GOCE User Workshop, Munich, Germany, 31 March - 1 April 2011, ESA SP-696.

Bratfisch, R., Jentzsch, G., . Steffen, H., 2010. A 3D Moho depth model for the Tien Shan from EGM2008 gravity data: in Proceedings, 7th EGU General Assembly, Vienna, 05 February 2010.

Burov, E.B., Diament, M., 1995. The effective elastic thickness (*Te*) of continental lithosphere: What does it really mean?. Journal of Geophysical Research, 100(B3): 3905-3927.

Cahill, T., Isacks, B.. 1992, Seismicity and shape of the subducted Nazca plate. Journal of Geophysical Research, 97(B12): 17503-17529.

Carter, W.D., 1974. Evaluation of ERTS-1 data: Applications to geologic mapping of S. America, with emphasis on the Andes mountain region, open file report, U.S. Geological Survey, Reston, Va.

Chapman, C.A., 1952: A new quantitative method of topographic analysis: American Journal of Science, 250: 428-452.

Chemeda, A., Lameland, S., Bokun, A., 2000. Strain partitioning and interpolate friction in oblique subduction zones: Constraints provided by physical modeling. Journal of Geophysical Research, 105: 5567-5582.

Cloos, M., 1992. Thrust-type subduction-zone earthquake and seamount asperities: A physical model for seismic rupture. Geology, 20: 601-604.

Coira, B., Kay, S.M., 1993. Implications of Quaternary volcanism at Cerro Tuzgle for crustal and mantle evolution of the Puna Plateau, Central Andes, Argentina. Contributions to Mineralogy and Petrology, 113(1): 40-58

Comte, D., Haessler, H., Louis, D., Pardo, M., Monfret, T., Lavenu, A., Pontoise, B., Hello, Y., 2002. Seimicity and stress distribution in the Copiapó, northern Chile subduction zone using combined on- and off-shore seismic observations. Physics of the Earth and Planetary Interiors, 123: 197-217.

Contreras-Reyes, E., Carrizo, D., 2011. Control of high oceanic features and subduction channel on earthquake ruptures along the Chile–Peru subduction zone. Phys. Earth Planet. Int. 186, 49–58.

DeMets, C., Gordon, R.G., Argus, D.F., Stein, S., 1990. Current plate motions: Geophysical Journal International, 101: 425-478.

DeMets, C., Gordon, R.G., Argus, D.F., Stein, S., 1994. Effect of the recent revisions to the geomagnetic reversal time scale on estimates of current plate motions. Geophysical Research Letters, 21: 2191-2194.

DeMets, C., Gordon, R.G., Argus, D.F., 2010. Geologically current plate motions. Geophys. J. Int., 181: 1-80

Ebbing, J., Braitenberg, C., Wienecke, S., 2007. Insights into the lithospheric structure and tectonic setting of the Barents Sea region from isostatic considerations. Geophysical Journal International, 171: 1390-1403.

EHB-Catalog, 2009. International Seismological Centre, EHB Bulletin, http://www.isc.ac.uk, Thatcham, United Kingdom, 2009.

Engdahl, E.R., van der Hilst, R., Buland, R., 1998. Global teleseismic earthquake relocation with improved travel times and procedures for depth determination. Bulletin of the Seismological Society of America, 88: 722-743.

Fernandez Seveso, F., Tankard, A., 1995. Tectonics and stratigraphy of the late Paleozoic Paganzo Basin of western Argentina and its regional implications, in: Tankard, A.J., Suárez Soruco, R., and Welsink, H.J., eds., Petroleum basins of South America: American Association of Petroleum Geologists, Memoria, p. 285-301. Tulsa.

Ferraccioli, F., Finn, C.A., Jordan, T.A., Bell, R.E., Anderson, L.M., Damaske, D., 2011. East Antarctic rifting triggers uplift of the Gamburtsev Mountains. Nature, 479: 388-392, doi:10.1038/nature10566.

Folguera, A., Ramos, V.A., 2011. Repeated eastward shifts of arc magmatism in the Southern Andes. A revision to the long term pattern of Andean uplift and magmatism. Journal of South American Earth Sciences, 32: 531- 546.

Gatti, A., Reguzzoni, M., Venuti, G., 2013. The height datum problem and the role of satellite gravity models. Journal of Geodesy, 87: 15-22. DOI: 10.1007/s00190-012-0574-3

Gerth, H., 1955. Der geologische Bau der sudamerikanischen Kordillere, Borntraeger, Berlin.

Gimenez, M.E., Martínez, M.P., Introcaso, A., 2000. A Crustal Model based mainly on Gravity data in the Area between the Bermejo Basin and the Sierras de Valle Fértil-Argentina. Journal of South American Earth Sciences, 13(3): 275-286.

Gimenez, M.E., Braitenberg, C., Martinez, M.P., Introcaso, A., 2009. A Comparative Analysis of Seismological and Gravimetric Crustal Thicknesses below the Andean Region with Flat Subduction of the Nazca Plate. Hindawi Publishing Corporation International, Journal of Geophysics, Article ID 607458, 8 p. doi:10.1155/2009/607458

Global CMT Project, 2006. Global CMT Web Page, in University, L.-D.E.O.o.C., Lamont-Doherty Earth Observatory of Columbia University: Lamont-Doherty Earth Observatory of Columbia University, Lamont-Doherty Earth Observatory of Columbia University, v. 2008, no. March 11.

Göetze, C., Evans, B., 1979. Stress and temperature in the bending lithosphere as constrained by experimental rock mechanism. Geophysical Journal of the Royal Astronomical Society, 59: 463-478.

González-Ferrán, O., Baker, P.E., Rex, D.C., 1985. Tectonic-volcanic discontinuity at latitude 27º South, Andean Range, associated with Nazca plate subduction. Tectonophysics, 112: 423-441.

Grombein, T., Heck, B., Seitz, K., 2010. Untersuchungen zur effizienten Berechnung topographischer Effekte auf den Gradiententensor am Fallbeispiel der Satellitengradiometriemission GOCE, Karlsruhe Institute of Technology, KIT Scientific Reports 7547, ISBN 978-3-86644-510-9, pp. 1-94.

Grombein, T., Heck, B., Seitz, K., 2013. Optimized formulas for the gravitational field of a tesseroid. Journal of Geodesy, 87: 645-600.

Guth, P.L., 1995. Slope and aspect calculations on gridded digital elevation models: Examples from a geomorphometric toolbox for personal computers. Zeitschrift fur Geomorphologie N.F. Supplementband 101, p.31-52

Guth, P.L., 1999. Quantifying and visualizing terrain fabric from digital elevation models, in Diaz, J., Tynes, R., Caldwell, D., and Ehlen, J., eds., International Conference on GeoComputation, 4th, Fredericksburg VA, Mary Washington College, 25-28 July, GeoComputation 99: CD-ROM ISBN 0- 9533477-1-0; http://www.geovista.psu.edu/geocomp/geocomp99/Gc99/096/gc_096.htm. (DEMbased classific. on elev., 'ruggedness', & topo fabric (fr. eigen-analysis))

Guth, P.L., 2007. MICRODEM home page: accessed 29 April 2007. http://www.usna.edu/Users/oceano/pguth/website/microdem.htm

Gutscher, M.A., 2000. An Andean model of interplate coupling and strain partitioning applied to the flat subduction of SW Japan (Nankai Trough). Tectonophysics, 333(1-2): 95-109.

Gutscher, M.A., Olivet, J.L., Aslanian, D., Maury, R., Eissen, J.P., 1999a. The 'lost Inca Plateau': Cause of flat subduction beneath Peru?. Earth and Planetary Science Letters, 171: 335-341.

Gutscher, M., Malavielle, J., Lallemand, S.E., Collot, J.Y., 1999b. Tectonic segmentation of the north Andean Margin: Impact of the Carnegie Ridge collision. Earth and Planetary Science Letters, 168: 255-270.

Gutscher, M.A., Spakman, W., Bijwaard, H., Engdahl, E.R., 2000. Geodynamics of flat subduction: Seismicity and tomographic constraints from the Andean margin. Tectonics, 19(5): 814-833.

Hackney, R.I., Echtler, H., Franz, G., Götze, H.J., Lucassen, F., Marchenko, D., Melnick, D., Meyer, U., Schmidt, S., Tazárová, Z., Tassara, A., Wienecke, S., 2006. The segmented overriding plate and coupling at the south-central Chile margin (36-42°S), in: Oncken, O., Chong, G., Franz, G., Giese, P., Götze, H.J., Ramos, V.A., Strecker, M.R. and Wigger, P., eds, The Andes: active subduction orogen, Frontiers in Earth Sciences, v. 1, Springer Verlag, p. 355-374.

Heck, B., Seitz, K., 2007. A comparison of the tesseroid, prism and point mass approaches for mass reductions in gravity field modeling. Journal of Geodesy, 81(2): 121-136. doi:10.1007/s00190-006-0094-0.

Hirt, C., Kuhn, M., Featherstone, W.E., Göttl, F., 2012. Topographic/isostatic evaluation of new-generation GOCE gravity field models. Journal of Geophysical Research, 117(B05407).

Hofmann-Wellenhof, B., Moritz, H., 2006. Physical Geodesy, 2nd edn, Springer, Berlin, 286pp.

Introcaso, A., Pacino, M.C., Guspi, F., 2000. The Andes of Argentina and Chile: Crustal configuration, Isostasy, Shortening and Tectonic features from Gravity Data. Temas de Geociencia, 5: 31.

James, D.E., Sacks, S., 1999. Cenozoic formation of the Central Andes: A geophysical perspective, in Skinner, B. et al. eds., Geology and Mineral Deposits of Central Andes: Special Publication of the Society of Economic Geology, London, 7: 1-25.

Janak, J., Sprlak, M., 2006. New Software for Gravity Field Modelling Using Spherical Armonic. Geodetic and Cartographic Horizon, 52: 1-8 (in Slovak).

~~Jordan, T.E., Allmendinger, R., 1986. The Sierras Pampean of Argentina: a modern analogue of Rocky Mountain foreland deformation. American Journal of Science, 286: 737-764.~~

Jordan, T.E., Isacks, B., Allmendinger, R., Brewer, J., Ramos, V.A., Ando, C.J., 1983a. Andean tectonics related to geometry of the subducted Nazca Plate. Geological Society of America Bulletin, 94(3): 341-361.

Jordan, T. E., Isacks, B., Ramos, V.A., Allmendinger, R., 1983b. Mountain building in the Central Andes. Episodes, 3: 20-26.

Kay, S. M., Abbruzzi, J.M., 1996. Magmatic evidence for Neogene lithospheric evolution of the central Andean “flat-slab” between 30ºS and 32ºS. Tectonophysics, 259: 15-28.

Kay, S.M., Coira, B., 2009. Shallowing and steepening subduction zones, continental lithospheric loss, magmatism, and crustal flow under the Central Andean Altiplano-Puna Plateau, in Kay, S., Ramos, V.A. and Dickinson, W., eds., Backbone of the Americas: Shallow subduction plateau uplift and ridge and terrane collision: Geological Society of America, Memoir 204, p. 229-259.

Kay, S., Coira, B., Mpodozis, C., 2008. Field trip guide: Neogene evolution of the Central Andean Puna plateau and southern Central Volcanic Zone, in Kay, S. and Ramos, V.A., eds., Field trip guides to the Backbone of the Americas: Shallow subduction plateau uplift and ridge and terrane collision: Geological Society of America, Field Trip Guide 13, p. 117-181.

Kay, S.M., Maksaev, V., Moscoso, R., Mpodozis, C., Nasi, C., Gordillo, C.E., 1988. Tertiary Andean magmatism in Chile and Argentina between 28 and 33ºS: correlation of magmatic chemistry with a changing Benioff zone. Journal of South American Earth Science, 1: 21-38.

Kay, S.M., Mpodozis, C., Ramos, V.A., Munizaga, F., 1991. Magma source variations for mid-late Tertiary magmatic rocks associated with a shallowing subduction zone and thickening crust in the Central Andes (28-33ºS), in Harmon, R.S., Rapela, C.W., eds., Andean Magmatism and its Tectonic Setting. Special Paper of the Geological Society of America, 26: 113-137.

Kay, S.M., Coira, B.L., Caffe, P.J., Chen, C.H., 2010, Regional chemical diversity, crustal and mantle sources and evolution of the Neogene Puna plateau ignimbrites of the Central Andes, J. Volcanol. Geotherm. Res., 198, 81-111.

Kendrick, E., Bevis, M., Smalley, R., Brooks, B., Barriga, R., Lauri, E., 2003. The Nazca – South America Euler vector and its rate of change. Journal of South American Earth Science, 16, p: 125-131.

Koike, K., Nagano, S., Kawaba, K., 1998. Construction and analysis of interpreted fracture planes through combination of satellite-image derived lineaments and digital terrain elevation data. Computers and Geosciences, 24(6): 573-584.

Kokogian, D.A., Seveso, F.F., Mosquera, A., 1993. Las secuencias sedimentarias triásicas, in: Ramos, V.A., et al. eds: Geología y Recursos Naturales de Mendoza. XII Congreso Geología Argentina y II Congreso de Exploración de Hidrocarburos. Relatorio I (7): 65-78 p, Mendoza.

Köther N., Götze, H.J., Gutknecht, B.D., Jahr, T., Jentzsch, G., Lücke, O.H., Mahatsente, R., Sharm, R., Zeumann, S., 2012. The seismically active Andean and Central American margins: Can satellite gravity map lithospheric structures?. Journal of Geodynamics, 59-60: 207-218, DOI:10.1016/j.jog.2011.11.004.

Kraemer, B. Adelmann, D. Alten M., Schnurr, W., Erpenstein, K. Kiefer, E., van den Bogaard, P., Görler, K., 1999. Incorporation of the Paleogene foreland into the Neogene Puna plateau: The Salar de Antofalla area, NW Argentina. Journal of South American Earth Sciences, 12: 157-182.

Lamb, S., Davis, P., 2003. Cenozoic climate change as a possible cause for the rise of the Andes. Nature, 425: 792-797.

Li, X., 2001. Vertical resolution: gravity versus vertical gravity gradient. The Leading Edge, 20(8): 901-904.

Li, Y., Braitenberg, C., Yang, Y., 2013. Interpretation of gravity data by the continuous wavelet transform: The case of the Chad lineament (North-Central Africa). Journal of Applied Geophysics, 90; 62-70.

Lowry, A.R., Ribe, N.M., Smith, R.B., 2000. Dynamic elevation of the Cordillera, western United States. Journal of Geophysical Research, 105(B10): 23-371.

Lyon-Caen, H., Molnar, P., 1983. Constraints on the structure of the Himalayan from an analysis of gravity anomalies and a flexural model of the lithosphere. Journal of Geophysical Research, 88: 8171-8191.

Mariani, P., Braitenberg, C., Ussami, N., 2013. Explaining the thick crust in Paraná basin, Brazil, with satellite GOCE gravity observations. Journal of South American Earth Sciences, 45: 209-223.

Marret, R., Allmendinger, R., Alonso, R., Drake, R., 1994. Late Cenozoic tectonic evolution of the Puna plateau and adjacent foreland, northwestern Argentine Andes. Journal of South American Earth Sciences, 7: 179-208.

Martinod, J., Husson, L., Roperch, P., Guillaume, B., Espurt, N., 2010. Horizontal subduction zones, convergence velocity and the building of the Andes. Earth and Planetary Science Letters, 299(3-4): 299-309.

Martinod, J., Guillaume, B., Espurt, N., Husson, L., Faccenna, C., Funiciello, F., Regard, V., 2013. Effect of aseismic ridge subduction on slab geometry and overriding plate deformation: Insights from analogue modeling. Tectonophysics, 588: 39-55. http://dx.doi.org/10.1016/j.tecto.2012.12.010

~~McGeary, S., Nur, A., Ben-Avraham, Z., 1985. Spatial gaps in arc volcanism: The effect of collision or subduction of oceanic plateaus. Tectonophysics, 119: 195-221.~~

~~Milana, J.P., Alcober, O., 1994. Modelo tectosedimentario de la cuenca triásica de Ischigualasto (San Juan, Argentina). Revista de la Asociación Geológica Argentina,49: 217-235.~~

Miranda, S., Robles, J.A., 2002. Posibilidades de atenuación cortical en la cuenca Cuyana a partir del análisis de datos de gravedad. Revista de la Asociación Geológica Argentina, 57(3): 271-279. ISSN 0004-4822.

Molodensky M.S., 1945. Fundamental problems of geodetic geavimetry. Trudy TsNIIGAIK, 42, Geodezizdat, Moscow, Russia (in Russian).

Molodensky M.S., Yeremeev V.F., Yurkina, M.I., 1962. Methods for study of the externalgravitational field and figure of the Earth: TRUDY Ts NIIGAiK, v. 131, Geodezizdat, Moscow,Russia (English translat.: Israel Program for Scientific Translation, Jerusalem 1962).

Mon, R., 1976. La tectónica del borde oriental de los Andes en las provincias de Salta, Tucumán y Catamarca, Republica Argentina. Revista de la Asociacion Geologica Argentina, 31(1): p. 65-72.

Montero Lopez, M.C. 2009. Estructura y magmatismo neógeno-cuaternario en la Sierra de San Buenaventura (Catamarca): su vinculación con la terminación austral de la Puna. Tesis Doctoral. Universidad Nacional de Salta (Unpublished), p. 271, Salta Argentina.

Montero López, M.C., Hongn, F., Brod, J. A., Seggiaro, R., Marrett, R.. Sudo, M., 2010a. Magmatismo ácido del Mioceno Superior-Cuaternario en el área de Cerro Blanco-La Hoyada, Puna Sur. Revista de la Asociación Geológica Argentina, 67(3): 329-348.

Montero López, M.C., Hongn, F., Seggiaro, R., Brod, J.A., Marrett, R., 2010b. Estratigrafía y geoquímica del volcanismo de composición intermedia (Mioceno superior-Plioceno) en el extremo oriental de la Cordillera de San Buenaventura (Puna Austral). Revista de la Asociación Geológica Argentina, 67(1): 63-80.

Montero, C., Guzmán, S., Hongn, F., 2011. Ignimbritas de la quebrada del río Las Papas (Cordillera de San Buenaventura, Catamarca): una primera aproximación petrológica y geoquímica. Acta geológica, 23(1-2): 78-93.

Mpodozis, C., Kay, M.S., 1992. Late Paleozoic to Triassic evolution of the Gondwana margin: Evidence from Chilean Frontal Cordilleran Batholiths (28°–31°S). Geological Society of America Bulletin, 104: 999-1014.

Mpodozis, C., Kay, S.M., Gardeweg, M., Coira, B., 1996. Geología de la región de Ojos del Salado (Andes centrales, 27ºS): implicancias de la migración hacia el este del frente volcánico Cenozoico Superior, in Proceedings, XIII Congreso Geológico Argentino, Asociación Geológica Argentina, Buenos Aires, Argentina, v. 3, p. 539-554.

Mulcahy, P., Chen, C., Kay, S., Brown, L., Isacks, B., Sandvol, E., Heit, B., Yuan, X., Coira, B., 2014. Central Andean Mantle and Crustal Seismicity under the Southern Puna plateau and Northern Margin of the Chilean Flatslab. Tectonics, in press. doi: 10.1002/2013TC003393

Müller, R.D., Roest, W.R., Royer, J.Y., Gahagan, L.M., Sclater, J.G. 1997. Digital isochrons of the world's ocean floor. J. Geophys. Res., 102, 3211–3214.

Müller, R.D., Sdrolias, M., Gaina, C., Roest, W.R., 2008. Age, spreading rates, and spreading asymmetry of the world's ocean crust. Geochemistry Geophysics Geosystems, 9: 18-36.

Oldenburg, D. 1974. The inversion and interpretation of gravity anomalies. *Geophysics*, 39, 526- 536.

Pail, R., Bruinsma, S. Migliaccio, F., Foerste, C., Goiginger, H., Schuh, W.D., Hoeck, E., Reguzzoni, M., Brockmann, J.M., Abrikosov, O., Veicherts, M., Fecher, T., Mayrhofer, R., Krasbutter, I., Sanso, F., Tscherning, C.C., 2011. First GOCE gravity field models derived by three different approaches. Journal of Geodesy, 85(11): 819-843.

Pardo, M., Comte, D., Monfret, T., 2002. Seismotectonic and stress distribution in the central Chile subduction zone. Journal of South American Earth Sciences, 15: 11-22.

Pavlis, N.K., Holmes, S.A., Kenyon, S.C., Factor, J.K., 2008. An Earth Gravitational Model to Degree 2160: EGM2008, in Proceedings, General Assembly of the European Geosciences Union: Vienna, Austria, 2008.

Pavlis, N.K., Holmes, S.A., Kenyon, S.C., Factor, J.K., 2012. The development and evaluation of the Earth Gravitational Model 2008 (EGM2008). Journal of Geophysical Research, 117(B04406). doi:10.1029/2011JB008916.

Pike, R.J., Acevedo, W., Card, D.H., 1989. Topographic grain automated from digital elevation models, in Proceedings, 9th International Symposium on Computer Assisted Cartography: Baltimore, April 2-7, 1989, ASPRS/ACSM, p.128-137.

Pilger, R.H., 1981. Plate reconstructions, aseismic ridges, and low-angle subduction beneath the Andes. Geological Society of America Bulletin, 92: 448-456.

Pinet, N., Cobbold, P.R., 1992. Experimental insights into the partitioning of motion within zones of oblique subduction. Tectonophysics, 206: 371-388.

Pubellier, M., Cobbold, P.R., 1996. Analogue models for the transpressional docking of volcanic arcs in the western Pacific. Tectonophysics, 253: 33-52.

Raghavan, V., Wadatsumi, K., Masumoto, S., 1993. Automatic extraction of lineament information of satellite images using digital elevation data. Nonrenewable Resources, 2(2): 148-155.

Ramos, V.A., 2009. Anatomy and global context of the Andes: Main geologic features and the Andean orogenic cycle, in Kay, S.M., Ramos, V.A. and Dickinson, W., eds., Backbone of the Americas: Shallow Subduction, Plateau Uplift, and Ridge and Terrane Collision: Geological Society of America, Memoir 204, p. 31-65.

~~Ramos, V.A., Folguera, A., 2009. Andean flat subduction through time, in Murphy, B., Keppie, J., and Hynes, A., eds., Ancient orogens and modern analogues. Special Publication of the Geological Society of London, 327: 31–54.~~

Ramos, V.A., Munizaga, F., Kay, S.M., 1991. El magmatismo cenozoico a los 33ºS de latitud: Geocronologia y relaciones tectónicas. In Proceedings, 6º Congreso Geológico Chileno: Viña del Mar, Chile, Actas 1, 892-896.

~~Ramos, V.A., Cegarra, M., Cristallini, E.O., 1996. Cenozoic tectonics of the High Andes of west-central Argentina (30-36°S latitude). Tectonophysics, 259: 185-200.~~

Ramos, V.A., Cristallini, E.O., Perez, D., 2002. The Pampean flat-slab of the Central Andes. Journal of South American Earth Sciences, 15: 59-78.

Ranero, C., von Huene, R., Weinrebe, W., Reichert, C., 2006. Tectonic Processes along the Chile Convergent Margin. In: Oncken, O., Chong., G., Franz, G., Giese, P., Götze, H.J., Ramos, V.A., Strecker, M.R., and Wigger, P., eds., The Andes – Active Subduction Orogeny: Frontiers in Earth Science Series, Springer-Verlag, Berlin Heidelberg New York, p. 91-121.

Reguzzoni, M., Sampietro, D., 2010. An Inverse Gravimetric Problem with GOCE Data: in Proceedings, International Association of Geodesy Symposia, "Gravity, Geoid and Earth Observation", 135(5): 451-456, Springer-Verlag, DOI: 10.1007/978-3-642-10634-7_60

Risse, A., Trumbull, R.B., Coira, B., Kay, S., van den Bogaard, P., 2008. 40Ar/39Ar geochronology of mafic volcanism in the back-arc region of the southern Puna plateau, Argentina. Journal of South American Earth Sciences, 26 (1): 1–15.

Rosenbaum, G., Giles, D., Saxon, M., Betts, P., Weinberg, R., Duboz, C., 2003. Subduction of the Nazca Ridge and the Inca Plateau: Insights into the formation of ore deposits in Peru. Earth and Planettary Science Letters, 239: 18-32.

Rossello, E.A., Mozetic, M.E., Cobbold, P.R., de Urreiztieta, M., Gapais, D., 1996. El espolón Umango-Maz y la conjugación sintaxial de los Lineamientos de Tucumán y Valle Fertil, in Proceedings, 13º Congreso Geológico Argentino y 3º Congreso de Exploración de Hidrocarburos: Buenos Aires, Argentina, Actas 2, 187-194.

Rossello, E.A, Limarino, C.O, Ortiz, A., Hernández, N., 2005. Cuencas de los Bolsones de San Juan y La Rioja, in: Chebili, G., Cortiñas, J.S., Spalletti, L.A., Legarreta, L., and Vallejo, E.L., eds., Simposio Frontera Exploratoria de la Argentina: VI Congreso de Exploración y Desarrollo de Hidrocarburos, p. 147-173.

Rousse, S., Gilder, S., Farber, D., McNulty, B., Patriat, P., Torres, V., Sempere, T., 2003. Paleomagnetic tracking of mountain building in the Peruvian Andes since 10 My. Tectonics, 22(5): 1048, doi:10.1029/2003TC001508.

Rummel, R., Yi, W., Stummer, C., 2011. GOCE gravitational gradiometry. Journal of Geodesy, 85(11): 777-790, doi: 10.1007/s00190-011-0500-0, 2011.33

~~Sacks, I.S., 1983. The subduction of young lithosphere. Journal of Geophysical Research, 88(B4): 3355–3366.~~

Salfity, J.A., 1985. Lineamientos transversales al rumbo andino en el Noroeste Argentino, in Proceedings, 4th Congreso Geologico Chileno: Chile, Actas 2, p. 119-137.

Salfity, J.A., Monaldi, C.R., Marquillas, R., Alvarez, L., 2005. Región de la Puna, in Proceedings, VI Congreso de Exploración y Desarrollo de Hidrocarburos, Capitulo 2 Libro Fronteras Exploratorias de la Argentina, p. 77-96.

Salisbury, M.J., Jicha, B.R., de Silva, S.L., Singer, B.S., Jiménez, N.C., Ort, M.H. 2011. $^{40}Ar/^{39}Ar$ chronostratigraphy of Altiplano-Puna Volcanic Complex ignimbrites reveals the development of a major magmatic province. Geological Society of America Bulletin, v. 123, p. 821-840. doi:10.1130/B30280.1

Sandwell, D.T., and Smith, W.H.F., 1997, Marine gravity anomaly from Geosat and ERS-1 satellite altimetry: Journal of Geophysical Research, v. 102, p. 10039-10050

Scholtz, C.H., and Small, C., 1997, The effect of seamount subduction on seismic coupling: Geology, v. 25, no. 6, p. 487-490.

Scholtz, C.H., Small, C., 1997. The effect of seamount subduction on seismic coupling, *Geology*, 25(6), 487-490.

Segerstrom, K., Turner, J.C.M., 1972. A conspicuous flexure in regional structural trend in the Puna of northwestern Argentine, U.S. Geological Survey, Washington, Research, Professional Paper, 800-B: B205-B209.

Seggiaro, R., Hongn, F., Folguera, A. Clavero, J. 2000. Hoja Geológica 2769 - II. Paso de San Francisco. Boletín 294, Programa Nacional de Cartas Geológicas 1:250.000, SEGEMAR - Servicio Nacional de Geología y Minería Argentino, Instituto de Geología y Recursos Minerales, 52 p., Buenos Aires.

Siebel, W., Schnurr, W. B., Hahne, K., Kraemer, B., Trumbull, R. B., van den Bogaard, P., Emmermann, R., 2001. Geochemistry and isotope systematics of small-to medium-volume Neogene–Quaternary ignimbrites in the southern central Andes: evidence for derivation from andesitic magma sources. Chemical Geology, 171(3): 213-237.

Siebert, L., Simkin, T., 2002. Volcanoes of the World: an Illustrated Catalog of Holocene Volcanoes and their Eruptions, Smithsonian Institution, Global Volcanism Program Digital Information Series, GVP-3, (http://www.volcano.si.edu/world/).

Smalley, R., Isacks, B., 1987. A high resolution local network study of the Nazca Plate Wadati-Benioff Zone under Western Argentina. Journal of Geophysical Research, 92: 13903-13912.

Stauder, W., 1973. Mechanism and spatial distribution of Chilean earthquakes with relation to subduction of the oceanic plate. Journal of Geophysical Research, 78: 5033-5061.

Steffen, R., Steffen, H., Jentzsch, G., 2011. A three-dimensional Moho depth model for the Tien Shan from EGM2008 gravity data. Tectonics, 30(TC5019) doi:10.1029/2011TC002886

Stein, S., Wysession, M., 2003. An Introduction to Seismology, Earthquakes, and Earth Structure, 1st edn, Blackwell Publishing, Malden, MA.

Stewart, J., Watts, A.B., 1997. Gravity anomalies and spatial variations of flexural rigidity at mountain ranges. Journal of Geophysical Research, 102(B3): 5327-5352.

Tassara, A., 2005. Interaction between the Nazca and South American plates and formation of the Altiplano-Puna plateau. Review of a flexural analysis along the Andean margin (15º-34ºS). Tectonophysics, 399: 39–57.

Tebbens, S.F., Cande, S.C., 1997. Southeast Pacific tectonic evolution from early Oligocene to present. Journal of Geophysical Research, 102(B6): 12061-12084.

Tscherning, C.C., 1976. Computation of the second-order derivatives of the normal potential based on the representation by a Legendre series: Manuscripta Geodaetica v. 1, no. 1, p. 71–92.

Trumbull, R.B., Riller, U., Oncken, O., Scheuber, E., Munier, K., Hongn, F., 2006. The timespace distribution of Cenozoic arc volcanism in the Central Andes: a new data compilation and some tectonic considerations. In: Oncken, O., Chong, G., Franz, G., Giese, P., Götze, H.-J., Ramos, V.A., Strecker, M.R, Wigger, P. (Eds) The Andes – Active Subduction Orogeny. Frontiers in Earth Science Series, Springer-Verlag, Berlin, Heidelberg, New York, pp. 29-43.

Uieda, L., Ussami, N., Braitenberg, C.F., 2010. Computation of the gravity gradient tensor due to topographic masses using tesseroids, in Proceedings, Meet. Am. Suppl., Eos Trans., AGU, v. 91, no. 26, Abstract G22A-04

Urreiztieta, M., de 1996. Tectonique neogene et bassins transpressifs en bordure meridionale de l`Altiplano-Puna (27ºS), Nord-Ouest argentin. Memoires, Geosciences Rennes, pp 311, Rennes.

Urreiztieta, M. de, Gapais, D., Le Corre, C., Cobbold, P.R., Rossello, E.A., 1996. Cenozoic dextral transspression and basin developement at the southern edge of the Altiplano-Puna, northwestern Argentina. Tectonophysics, 254: 17-39.

Vening-Meinesz, F.A. 1939. Tables Fondamentales pour la Reduction Isostatique Regionale. Bulletin Géodésique 63: pp. 711-776

Vigny, C., Rudloff, A., Rueggb, J.C., Madariaga, R., Campos, J., Alvarez, M., 2009. Upper plate deformation measured by GPS in the Coquimbo Gap, Chile. Physics Earth and Planetary Interiors, 175: 86–95.

Viramonte, J.G., Arnosio, M., Becchio, R., de Silva, S., Roberge, J., 2008. Cerro Blanco Volcanic Complex, Argentina: A Late Pleistocene to Holocene rhyolitic arc –

related caldera complex in the Central Andes. IAVCEI, General assembly Reykjavík, Islandia.

Völker, D., Wiedicke, M., Ladage, S., Gaedicke, C., Reichert, C., Rauch, K., Kramer, W., Heubeck, C., 2006. Latitudinal Variation in Sedimentary Processes in the Peru-Chile Trench off Central Chile, in Oncken, O., Chong., G., Franz, G., Giese, P., Götze, H.J., Ramos, V.A., Strecker, M.R., and Wigger, P., eds., The Andes – Active Subduction Orogeny: Frontiers in Earth Science Series, Springer-Verlag, Berlin Heidelberg New York, p. 193-216

Von Huene, R., Corvalán, J., Flueh, E.R., Hinz, K., Korstgard, J., Ranero, C.R., Weinrebe, W., and CONDOR scientists, 1997. Tectonic control of the subducting Juan Fernández Ridge on the Andean margin near Valparaiso, Chile. Tectonics, 16(3): 474–488.

Watts, A., 2001. Isostasy and flexure of the Lithosphere: Cambridge University Press, 458.

Wessel, P., 1999. New Hotspotting tools released, in Proceedings, EOS Trans. AGU, v. 80, no. 29, p. 319.

Wessel, P., 2001. Global distribution of seamounts inferred from gridded Geosat/ ERS-1 altimetry. Journal of Geophysical Research, 106(B9): 19431-19441.

Wessel, P., 2008. Hotspotting: Principles and properties of a plate tectonic Hough transform. Geochemistry Geophysics Geosystems, 9(Q08004). doi:10.1029/2008GC002058.

Wessel, P., Kroenke, L.W., 1997. A geometric technique for relocating hotspots and refining absolute plate motions. Nature, 387: 365-369.

Wessel, P., Kroenke, L.W., 1998. The geometric relationship between hot spots and seamounts: implications for Pacific hot spots. Earth and Planetary Science Letters, 158: 1-18.

Wessel, P., Smith, W.H.F., 1998. New, Improved Version of the Generic Mapping Tools Released, in Proceedings, EOS Trans, AGU, v. 79, no. 47, p. 579.

Whittaker, J., Goncharov, A., Williams, S., Müller, R.D., Leitchenkov, G., 2013. Global sediment thickness dataset updated for the Australian-Antarctic Southern Ocean: Geochemistry Geophysics Geosystems. DOI: 10.1002/ggge.20181

Wienecke, S., 2002. Homogenisierung und Interpretation des Schwerefeldesentlang der SALTTraversézwischen 36º-42ºS: Unpublished Diploma Thesis, FreieUniversität, Berlin, Germany.

Wienecke, S., 2006. A new analytical solution for the calculation of flexural riidity: significance and applications: PhD Thesis, Free University Berlin, Berlin, 126 p. World Wide Web Address: http://www.diss.fuberlin.de/

Wienecke, S., Braitenberg, C., Göetze, H.J., 2007. A new analytical solution estimating the flexural rigidity in the Central Andes. Geophysics Journal International, 169: 789-794.

Wild-Pfeiffer, F., 2008. A comparison of different mass element for use in gravity gradiometry. Journal of Geodesy, 82: 637-653, doi 10.1007/s00190-008-0219-8.

Woodcock, N.H., 1977. Specification of fabric shapes using an eigenvalue method. Geological Society of America Bulletin, 88: 1231-1236.

Yáñez, G., Cembrano, J., 2004. Role of viscous plate coupling in thelate Tertiary Andean tectonics. Journal of Geophysical Research, 109. doi 10.1029/2003JB002494

Yañez, G.A., Ranero, C.R., von Huene, R., Diaz, J., 2001. Magnetic anomaly interpretation across the southern Central Andes (32°–34° S). The role of the Juan Fernandez Ridge in the late Tertiary evolution of the margin. Journal of Geophysical Research, Solid Earth, 106(B4): 6325–6345.

Yi W, Rummel R (2014) A comparison of GOCE gravitational models with EGM2008. J Geodyn 73: 14–22. http://dx.doi.org/10.1016/j.jog.2013.10.004.

Zadro, M., Braitenberg, C., 1997. Spectral Methods in gravity inversion: the geopotential field and it's derivatives. Annali di geofisica XL, v. 5, p. 1433-1443.

Zentilli, M., 1974. Geological evolution and metallogenic relationships in the Andes of northern Chile between 26º and 29º south, Ph.D. thesis, 446 pp., Queen's University, Kingston, Ont.

Zhou, R., Schoenbohm, L., Cosca, M., 2014. Recent, slow normal and strike-slip faulting in the Pasto Ventura region of the Southern Puna Plateau, NW Argentina. Tectonics. In Press.

APPENDIX A: Magmatic evolution of the southern Puna plateau

Over flat subduction settings, the volcanic arc migrates and expands through the foreland area and consequently thermal crustal structure changes, producing the shallowing of brittle-ductile transitions that favor shortening of the upper crust (see James and Sacks, 1999 and Kay and Coira 2009). In particular, the Chilean-Pampean flat subduction zone, initiated ~17 My ago, has been related to the exhumation of the foreland area through the activity of decollements inaugurated since the arc foreland excursion (see Ramos et al. (2002), for an extended discussion).

The volcanic centers within the Ojos del Salado-San Buenaventura volcanic lineament are affected and controlled by normal and right lateral neotectonic structures, defining a general ENE structural alignment (Fig. 3) (Kay et al. 2008; Marrett et al. 1994; Mpodozis et al. 1996; Seggiaro et al. 2000; Zhou et al. 2014). Most of the volcanic centers controlled by these structures are Pleistocene in age, although some show a more prolonged activity during the Holocene (Baker et al. 1987; Kraemer et al. 1999; Montero López, 2009; Mpodozis et al. 1996; Risse et al. 2008; Seggiaro et al. 2000; Viramonte et al. 2008). Based on radiometric ages compiled along the Ojos del Salado-San Buenaventura volcanic lineament, four magmatic stages (>8My, 8-4My, 4-2My and <1My) can be recognized with distinctive distributions across the arc and retroarc zones (Figs. A1 and A2).

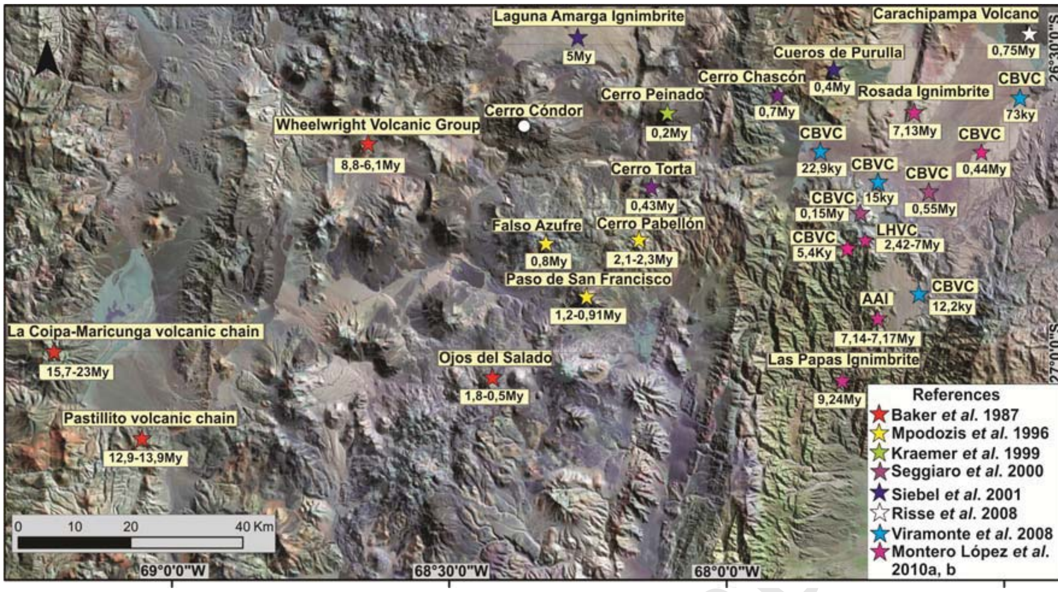

Figure A1. *Radiometric ages in volcanic centers along the Ojos del Salado-San Buenaventura volcanic lineament from the arc front to the eastern retroarc area, draped on top of a TM image (radiometric ages were compiled from Baker et al. 1987; Kraemer et al. 1999; Montero López, 2009; Mpodozis et al. 1996, Seggiaro et al. 2000; Risse et al. 2008; Viramonte et al. 2008).*

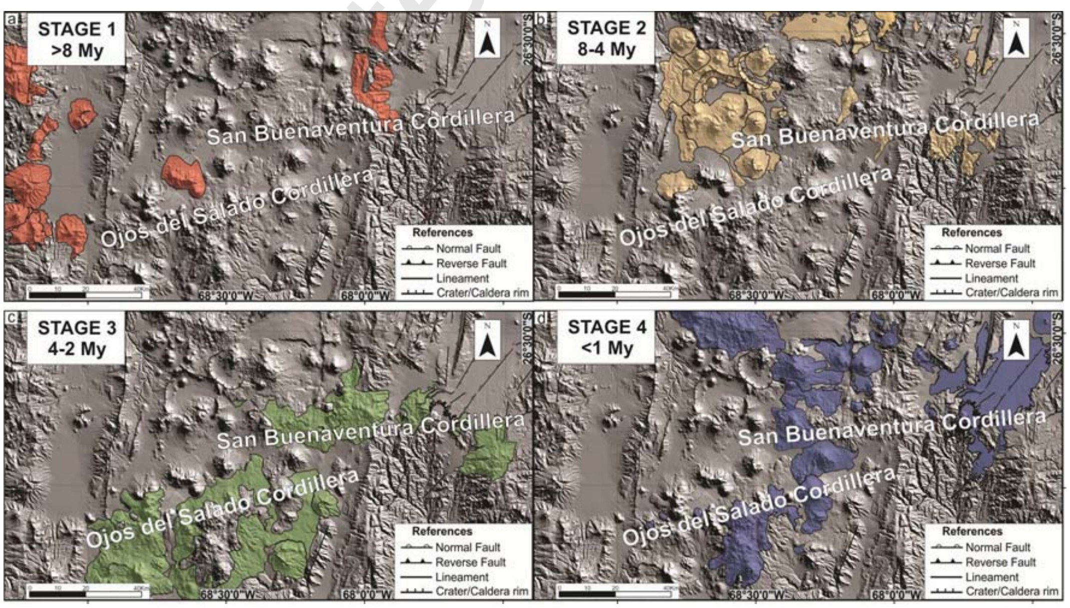

Figure A2. *Spatial and temporal distribution of volcanism in the Altiplano-Puna Plateau from the arc front to the retroarc area through the Ojos del Salado-San Buenaventura volcanic lineament (Coira y Kay 1993; Kay and Coira 2009; Kay et al. 2010; Salisbury et al. 2011; Trumbull et al. 2006).*

An older stage (>8My) is mainly represented on the Chilean Andean slope by La Coipa-Maricunga and Pastillito volcanic associations (Baker et al. 1987), represented by stratovolcanoes and domes associated with ignimbrite deposits with a general northward trend. In particular, the Pastillito volcanic association (12.9-13.9My) is developed 15-20 km east of previous volcanism in the region. At the end of this stage, the eastward migration of the volcanism is more evident (Kay and Coira, 2009), with middle to late Miocene volcanic centers located in the San Buenaventura volcanic lineament (Montero López et al. 2010a, 2011; Seggiaro et al. 2000). The 8-4 My stage comprises mainly riodacitic calderas with associated ignimbrites (e.g. Wheelwright caldera, Laguna Amarga Ignimbrite and Rosada Ignimbrite) and backarc andesitic volcanism of La Hoyada Volcanic Complex (Montero López et al. 2010b). The 4-2 My stage marks the onset of a different tectonic control with volcanic centers aligned through a NE trend (Baker et al. 1987). In this stage, the Peñas Blancas Volcanic group and the main volume of the San Buenaventura volcanic lineament was built. The last stage, <1My, is represented by the emplacement of a series of stratovolcanoes such as San Francisco, IncaHuasi, Falso Azufre, Ojos del Salado and Cóndor, and the Cerro Blanco Volcanic Complex towards the back arc region (Arnosio et al. 2008; Montero López et al. 2010a; Viramonte et al. 2008).

APPENDIX B: Statistical comparison between GOCE and EGM2008 models

Even though recent satellite gravity missions have gained an extraordinary improvement in the global mapping of the Earth gravity field, the models derived solely from data of these missions (e.g. Pail et al. 2011) present a lower spatial resolution than mixed satellite-terrestrial global models like EGM2008 (Pavlis et al. 2008). GOCE data were obtained through acceleration and gravity gradient measurements, and also through orbit monitoring. For degrees greater than N=120, EGM2008 relies entirely on terrestrial data, so GOCE only models, as the GO_CONS_GCF_2_TIM_R4 with N=250 (Pail et al. 2011), are a remarkably important independent quality assessment tool to control the quality of the terrestrial data entering in EGM2008 (Braitenberg et al. 2011a; Alvarez et al. 2012, 2014). A comparison analysis up to the maximum degree (N=250) of the GOCE model is a simple way to evaluate the contribution of the terrestrial data between N=120 and N=250 entering EGM2008. If the residual is small ground-based data represent accurately the field up to degree N=250 relying on the correctness for higher orders (see Braitenberg et al. 2011b; Alvarez et al. 2012). The errors of the original terrestrial data affect the errors of the EGM2008 values up to N=250, because the spherical harmonic expansion can be seen as an averaging process. The standard deviations between GOCE and EGM2008 thus represent varying quality of the original terrestrial data, because the quality of the GOCE data is locally homogeneous. Where the standard deviations are small, the original data must have been accurate or otherwise the same downscaled values and a small standard deviation would have been only obtained by chance (See Braitenberg et al. (2011a) and Alvarez et al. (2012) for a more detailed explanation). Yi and Rummel (2014) made a comparison of GOCE models with EGM2008 and found that the agreement between EGM2008 and the GOCE-models up to degree and order 200 is good, with a global (excluding the polar gaps of GOCE orbits, throughout) geoid RMS-difference of 11 cm in the ocean areas and between 8-20 cm in the continental areas. Therefore GOCE is a remarkably important independent quality assessment tool for EGM2008, especially in those areas where no precise terrestrial data are available in the EGM2008 model as is the case of vast parts of South America. Here, substantial differences are expected, especially in the Andes region where the topography is high and rough in many areas. An assessment for the comparison of terrestrial observations and EGM2008 and GOCE was made by Bomfim et al. (2013).

The absolute residual (Fig. B1) between the gravity anomaly derived from GOCE model (Pail et al. 2011) and the gravity anomaly derived from the EGM2008 model (Pavlis et al. 2008, 2012) shows that the fields are in partial agreement. Statistical parameters for the difference between the two fields are shown on Table B1. A high-quality region is compared with a low-quality region in terms of the residual histogram. An area with degraded quality, corresponding to the 2º x 2º black square in Fig. B1, is compared to a square of equal size (white) of relatively high quality.

Average difference	*0.0772 mGal*
Standard Deviation	*12.341 mGal*
Maximal value of difference	*62.021 mGal*

Table B1: *Statistical parameters for the difference.*

The histograms of the residuals (Fig. B2) illustrate the higher values for the black square and a limited error (+/−10 mGal) for the white square. Instead, the black square, presents a high error (−45/+35 mGal) with a uniform distribution.

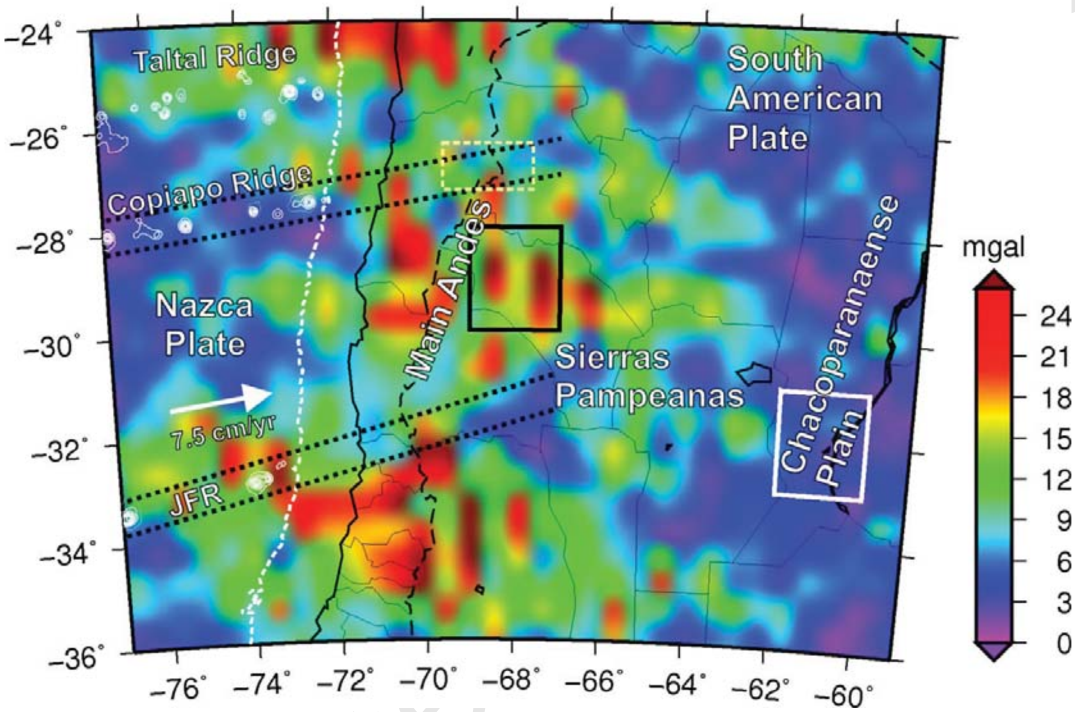

Figure B1. *Absolute difference between the two fields. The black square shows the area with erroneous data, while the white square shows the area with good data agreement. National borders: dashed black line; coastal borders: solid black line. The yellow dashed rectangle represents the approximate area where the deflection of the Andean structures was detected by means of the Ga and Tzz from EGM2008 model (Figs. 4a, b and 5b).*

The absolute difference between both fields shows a range of variation between approximately +6 mGal and +24 mGal in the area where the Andean structures were deflected (Figs. 4a, b and 5b) and detected by means of the Ga and Tzz from EGM2008 model (yellow dashed rectangle in fig B1). The gravity signal that shows such pattern reaching less than -450 mGal (Fig. 4b), thus giving a signal to noise ratio of approximately SNR≈24 mGal/ 450 mGal=0.05333.

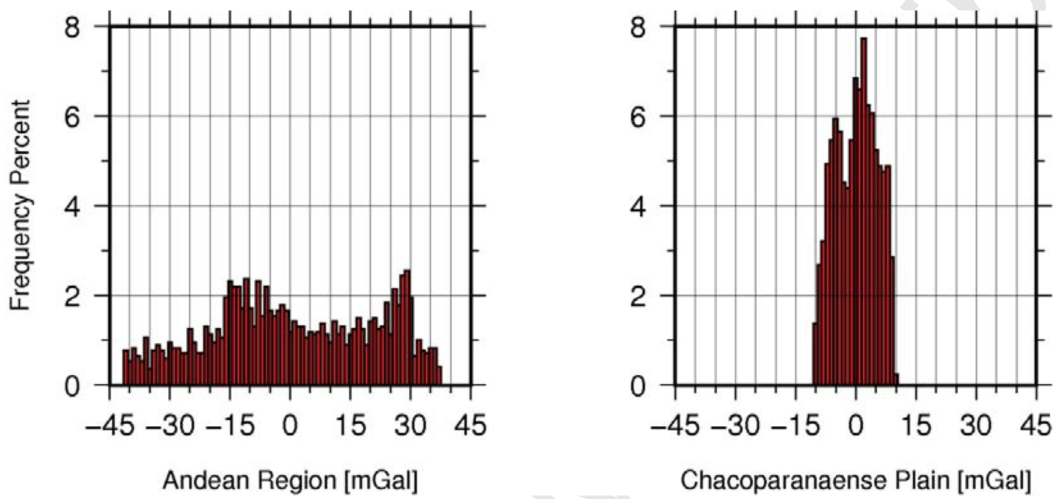

Figure B2. *Histogram of the residual gravity anomaly between EGM2008 and GOCE (up to degree and order N=250). Left (Good tile): white square of Fig. B1. Right (Bad tile): black square of Fig. B1.*

As a statistical measure of EGM2008 quality, the root mean square (rms) deviation from the mean was calculated, on sliding windows of 20’ x 20’. The result is shown on Fig. B3. The most frequent value of the rms deviation is 2 mGal (Fig. B4). The regions where the EGM2008 present higher differences of the rms difference, when compared to GOCE, reach up to 12.5 mGal. The locations where the terrestrial data present the main differences reflected up to 12 mGal. Approximately the 85.5% of the rms deviation is below 5 mGal.

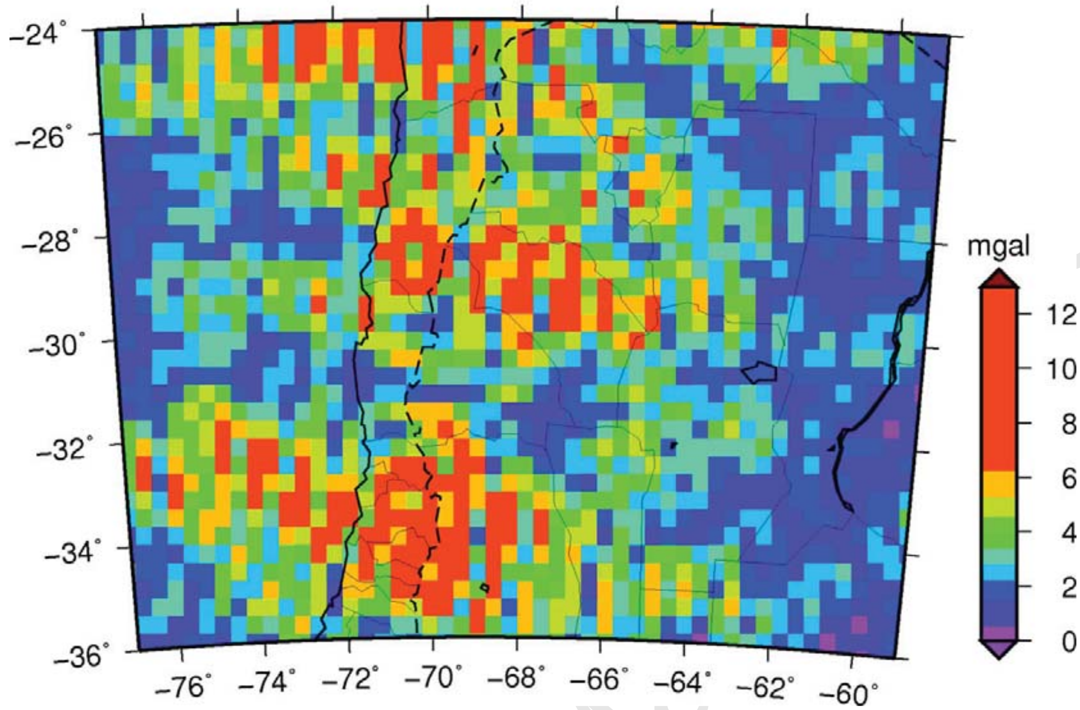

Figure B3. *Root mean square of the gravity residual on 20' x 20' tiles.*

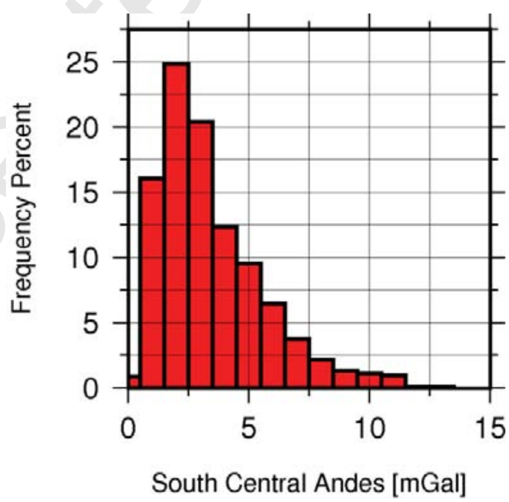

Figure B4. *Histogram of the rms deviations on 0.5º x 0.5º tiles.*

APPENDIX C: Calculation of the flexural strength of the lithosphere

To accomplish the inverse modeling of the flexural rigidity, we used Lithoflex software package (www.lithoflex.org). Isostatic modeling adopts the isostatic thin plate flexure model (e.g. Watts, 2001) and the use of a newly derived analytical solution for the 4th order differential equation that describes the flexure of a thin plate (concept introduced by Vening-Meinesz in 1939). This allows the analytical calculation of the deflection of a thin plate for any irregular shape of the topography (see Wienecke 2006 and references therein for a more detailed discussion). To estimate the elastic properties of the plate for a known load, a crustal load and the crust-mantle interface to be used as a reference surface are needed (Wienecke, 2006). The load acting on the crust is constituted by the combination of the overlying topography plus a density model (Braitenberg et al. 2007). A density variation within the crust represents a variation in the load, and must be reflected in the isostatic response (Ebbing et al. 2007). Long wavelength information of the gravity field mainly corresponds to the crust/mantle density contrast, but sedimentary basins can also produce a long wavelength signal thus influencing the correct gravity crust mantle interface estimation by gravity inversion process (Wienecke 2006). Therefore, the gravity effect of sediments was calculated in order to reduce the gravity data.

The topographic load or equivalent topography was calculated using topographic/bathymetric data from ETOPO1 (Amante and Eakins, 2009). The densities used for calculation were 1,030 kg/m^3 for water and 2,800 kg/m^3 for the crust. This method requires two input parameters: the density contrast and reference depth. Standard parameters such as normal crust thickness Tn = 35 km, and a crust mantle density contrast of -400 kg/m^3 were used. The Bouguer anomaly was calculated using the GOCE satellite data (GO_CONS_GCF_2_TIM_R4, http://icgem.gfz-potsdam.de/ICGEM/, Pail et al. 2011) up to degree/order N=250 and reduced by the effect of sediments.

Forward calculation of the gravity effect of the basin fillings (Fig. C1) was done taking into account a linear variation of density with depth (see Braitenberg et al. 2007). To perform this calculation we defined a two-layer reference model of the continental crust with an upper crustal density of 2,700 kg/m^3 and a lower crustal density of 2,900 kg/m^3. To perform this operation we used the bathymetry from ETOPO1 (Amante and Eakins, 2009) and off-shore sediment thicknesses from Whittaker et al. (2013). On-shore basins were modeled using depths to the top of the basement calculated from gravimetric studies and seismic lines of Yacimientos Petroliferos Fiscales (YPF), Texaco, Repsol YPF, YPF S.A. and OIL M&S, and from Barredo et al. (2008); Fernandez Seveso and Tankard (1995); Kokogian et al. (1993), Milana and Alcober (1994), Miranda and Robles (2002), Rosello et al. (2005) and Gimenez et al. (2009). The correction amounts up to -45 mGal for the main on-shore basins and up to a few mGal for oceanic sediments reaching their maximum over the Chilean trench.

Masses above sea level	ρ_s	2,670 kg/m^3
Upper crustal density	ρ_{uc}	2,700 kg/m^3
Lower crustal density	ρ_{lc}	2,900 kg/m^3
Upper mantle density	ρ_m	3,300 kg/m^3
Young modulus	E	10^{11} N/m^2
Poisson ratio	Σ	0.25

Table C1: *Parameters used in the flexural modeling.*

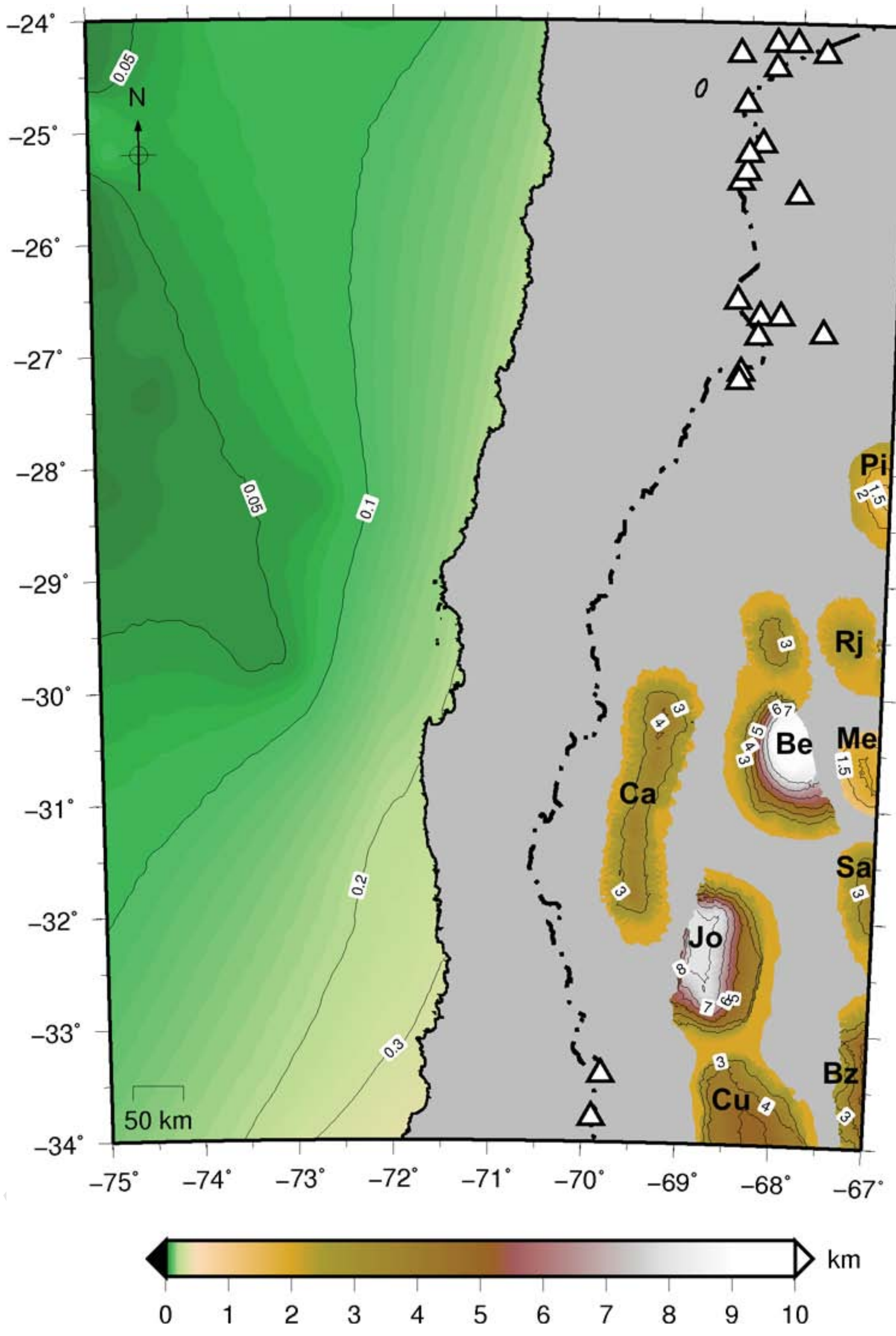

Figure C1. *Sediment thicknesses used to reduce the gravity data. Offshore sediment thickness is from Whittaker et al. (2013). The basins over the South American plate were approximated using gravity databases and basement depths from seismic lines*

(YPF S.A. unpublished report). Sedimentary basins: Be, Bermejo; Jo, Jocoli; Sa, Salinas; Cu, Cuyana; Bz, Beazley, Ca, Calingasta; Pi, Pipanaco; Rj, La Rioja; Me, Medanos.

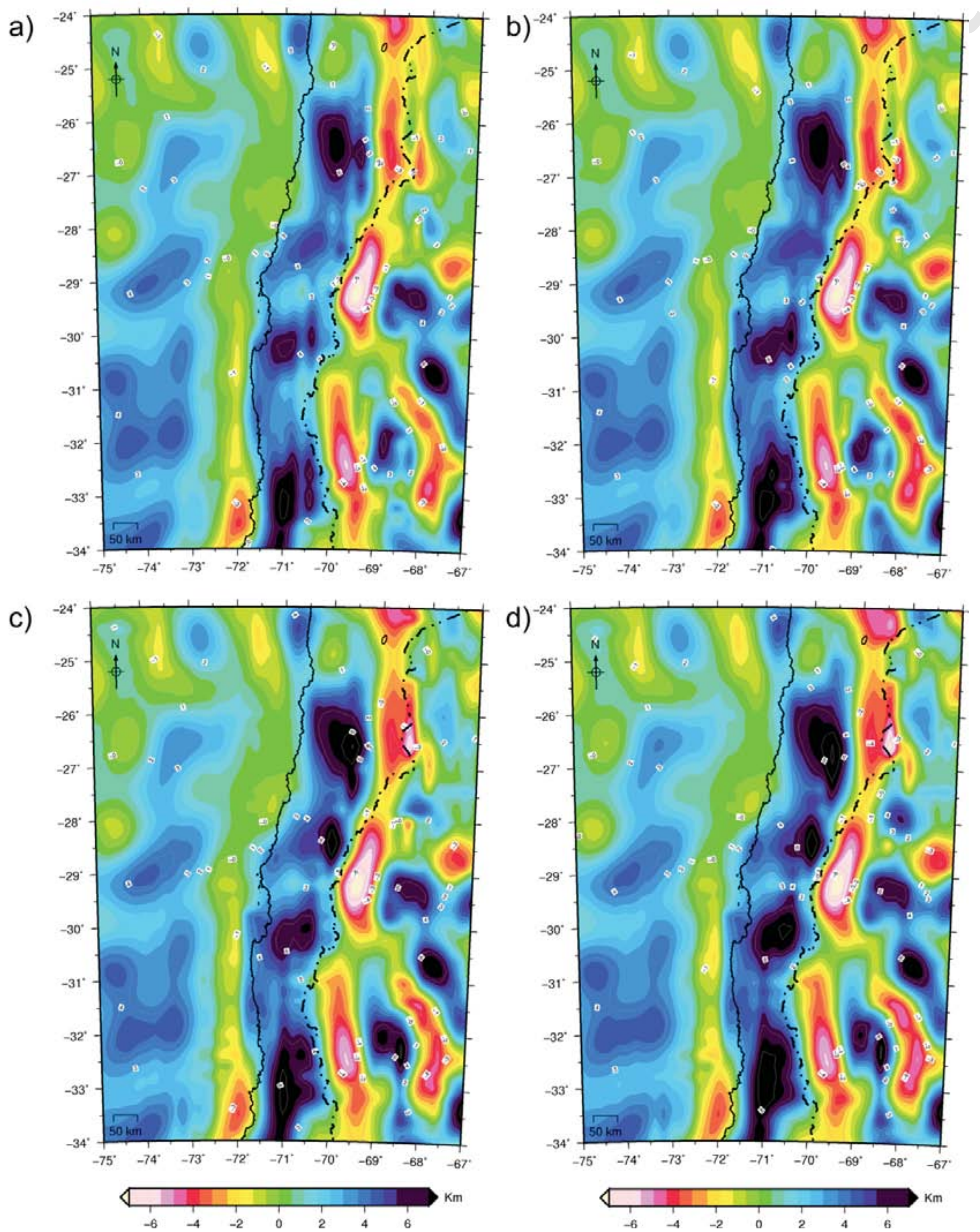

Figure C2. *Residual obtained by subtracting the crust–mantle interface obtained by gravity inversion of the sediment corrected Bouguer anomaly minus the crust–mantle interface obtained from the flexural model.* ***a)*** *Window size 60x60km.* ***b)*** *Window size 70x70km.* ***c)*** *Window size 80x80km.* ***a)*** *Window size 90x90km.*

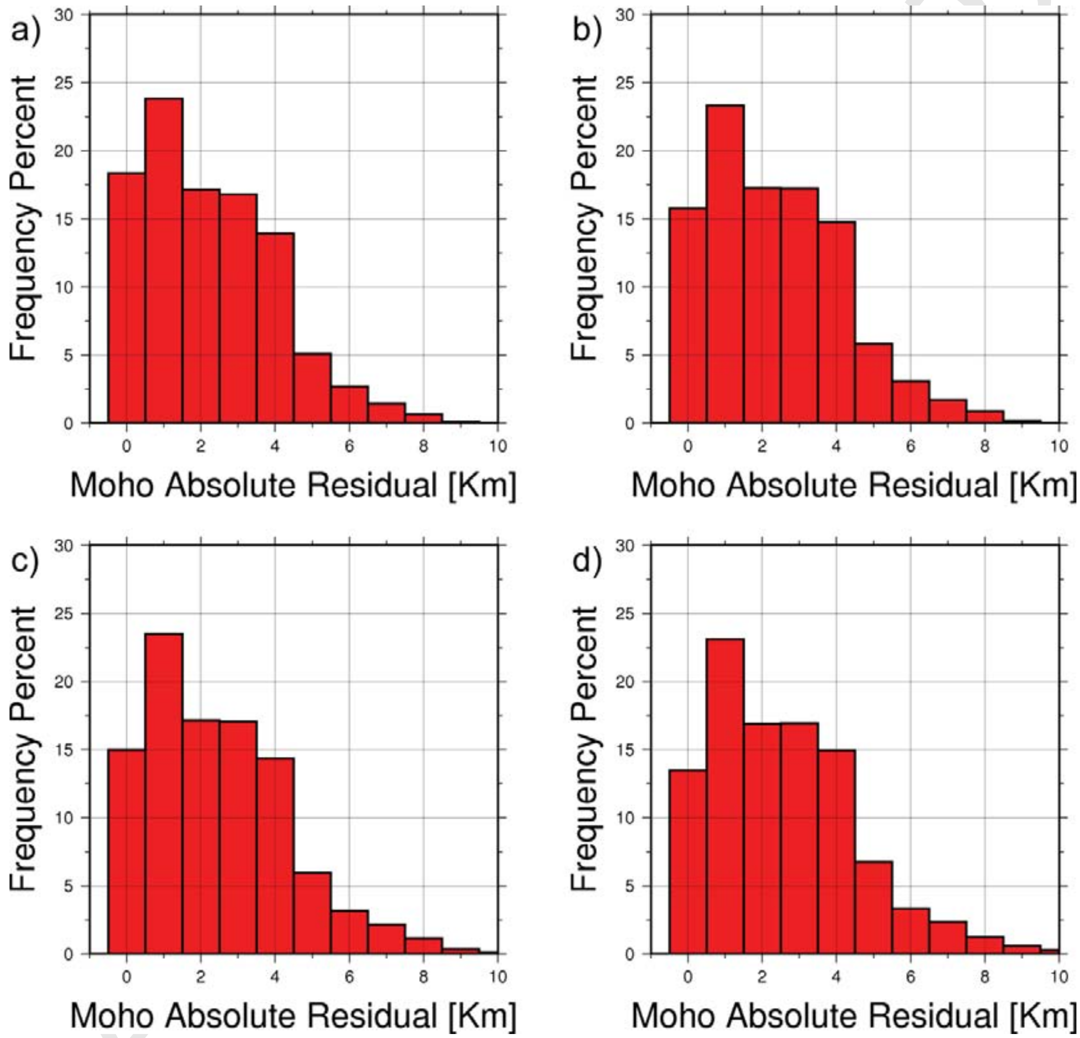

Figure C3. *Histogram of the residual Moho between the crust–mantle interface obtained by gravity inversion and the crust–mantle interface from the flexural model. Globally, more than 85% of the error is less than 4 km.* ***a)*** *Window size 60x60km (error ≈ 89% < 4 km).* ***b)*** *Window size 70x70km. (error ≈ 88% < 4 km)* ***c)*** *Window size*

80x80km (error ≈ 87% < 4 km) ***d)*** *Window size 90x90km (error ≈ 85% < 4 km). The residual obtained for the smaller window size of 60x60km shows a slight better fitting, and increasing error as window size increases. We selected the window size of 80x80km as is in the order of magnitude of the half wavelength of the resolution of GOCE model.*

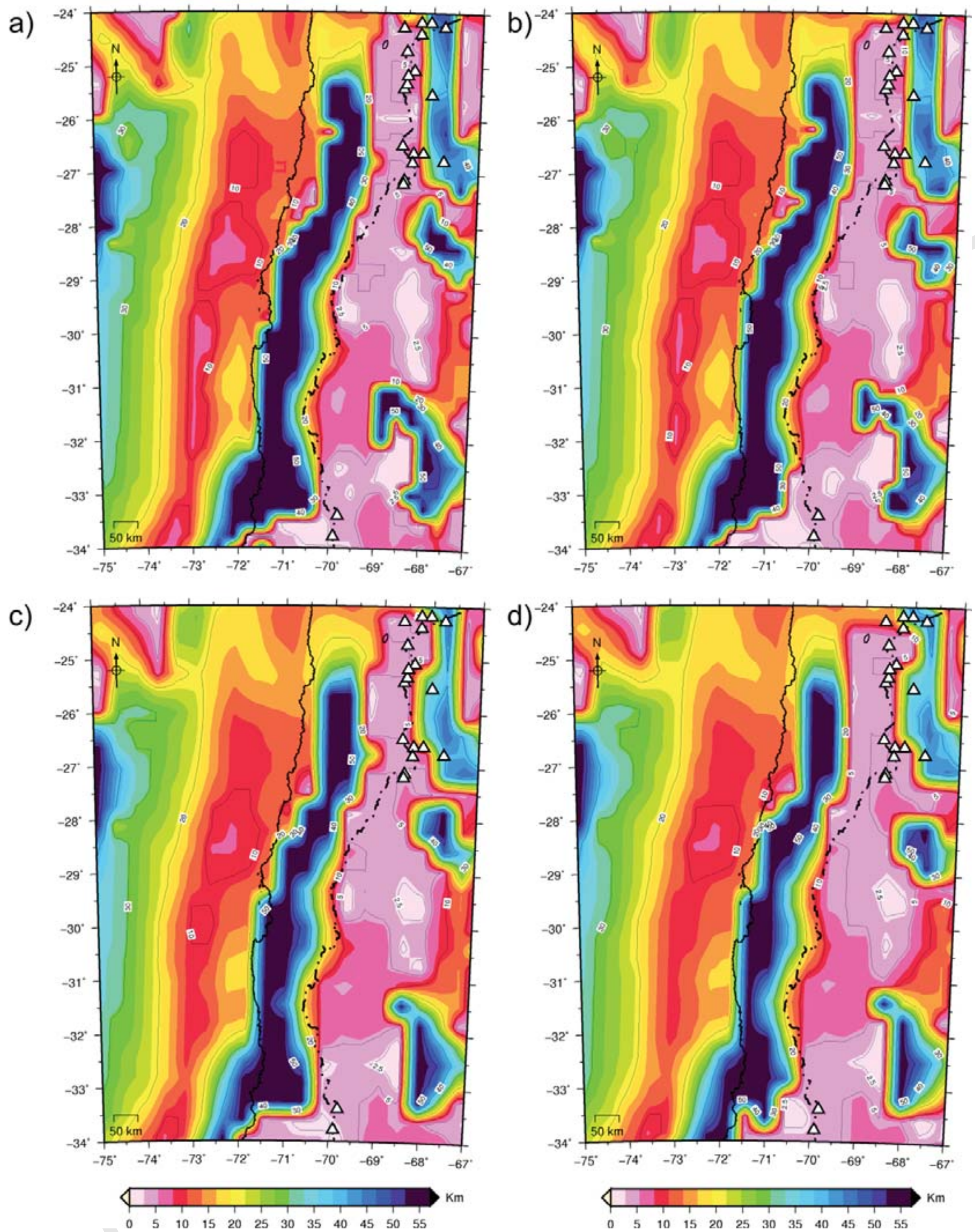

Figure C4. *Elastic thicknesses obtained from GOCE data for different window size of calculation.* ***a)*** *Window size 60x60km* ***b)*** *Window size 70x70km.* ***c)*** *Window size 80x80km* ***d)*** *Window size 90x90km.*

From the reduced Bouguer anomaly (Figure 6a) we estimated the gravimetric crust-mantle discontinuity (Figure 6b) by gravity inversion. This method uses an iterative algorithm that alternates downward continuation with direct forward modeling (Braitenberg et al. 1999) and is somewhat analogous to the Oldenburg-Parker inversion approach (Oldenburg 1974; see Braitenberg et al. 2007, for a detailed explanation).

The obtained crustal load (obtained from topo/bathymetry data and the density model) and the Moho undulations (obtained by inversion of the reduced Bouguer anomaly) were used for the inverse flexure calculation. The flexural rigidity was inverted in order to match the known loads with the known crustal thickness model (i.e. to model the gravity Moho in terms of an isostatic model). The elastic thickness was allowed to vary in the range of 1< Te < 55 km and was iteratively estimated over moving windows of 60 x 60 km, 70 x 70 km, 80 x 80 km and 90 x 90 km, size (Fig. C4). The model parameters are given in Table 1, where the adopted densities are standard values already used in the region under study by other authors (Gimenez et al. 2000, 2009; Introcaso et al. 2000; Miranda and Robles, 2002).

The residual between the Moho from gravity inversion and the flexure Moho is the residual Moho (Fig. C2). The Moho undulations obtained from gravity inversion agree with the CMI undulations expected for the flexural model, about 85 percent within 4 km of difference (Fig. C3). Positive values of the residual Moho indicate that the gravity Moho is shallower than the flexure Moho. The correction of the gravity and load effect of the sediments, allows gravity Moho to comply with load changes: once the negative effect on the Bouguer anomaly from the sediments is removed, the Moho from gravity inversion will be shallower and will follow the flexure Moho (Alvarez et al. 2015). Negative values of the residual Moho in the Main Andes indicate that the gravity Moho is deeper than the flexure Moho. The flexural model used in this work is a simplification and would be influenced by the stress of the down-going plate. Thus, the Te solutions along the active subduction margin could possibly be distorted (as explained by Braitenberg et al. 2007).

APPENDIX D: TERRAIN FABRIC ANALYSIS

The terrain fabric or grain (Pike et al. 1989) measures a point property of a digital elevation model (DEM) or any other field (in this case is applied to the Tzz), constituting an expression of the tendency to form linear features (Guth, 1999). Guth (1999) explained that eigenvector analysis reliably extracts the terrain fabric, both in strength and orientation. This analysis extracts eigenvectors and eigenvalues (S) from a 3 by 3 matrix of the sum of the cross products of the directional cosines of the surface perpendiculars at each point in the DEM (Guth, 1999). The dominant orientation is represented by the vector V1 that together with the vector V2 forms the main plane of the fabric, while V3 is normal to this plane. The eigenvalues S1, S2 and S3 express their normalized values. The ln(S2/S3) measure the fabric or grain, orientations of S2 and S3 define the dominant grain of the topography, and the ratio S2/S3 determines the strength of the grain. The eigenvalue method was discussed by Woodcook (1977) for the representation of fabric shapes in structural geology, paleomagnetism, sedimentology and glaciology. This method is used to quantify Chapman's (1952) technique in Microdem software (Guth, 1995, 2007).

APPENDIX E: Gravity derived profiles

Five profiles (Fig. E1) were traced perpendicularly to the Copiapó ridge track (for location see Fig. 5b) for the *Tzz* and *Ga* from EGM2008 and for Moho and Te from GOCE. While profiles P1 and P2 were traced over the Copiapó ridge in an offshore position, profiles P3, P4 and P5 were traced cutting across the Ojos del Salado-San Buenaventura volcanic lineament (Fig. 5b). The bathymetric expression of the Copiapó ridge (P1, P2) is expressed by high values of *Tzz* and *Ga*. Similarly, inland, the topographic highs along the ridge path (P3, P4, P5) are also reflected by high values of *Tzz* and *Ga*. Even though the profile P5 does not show a significant topographic expression, a relatively high *Tzz* value was also obtained. The *Ga* (P5) shows a relative high too, although it is masked by the negative effect of the Andean root that is expressed by the low Moho values.

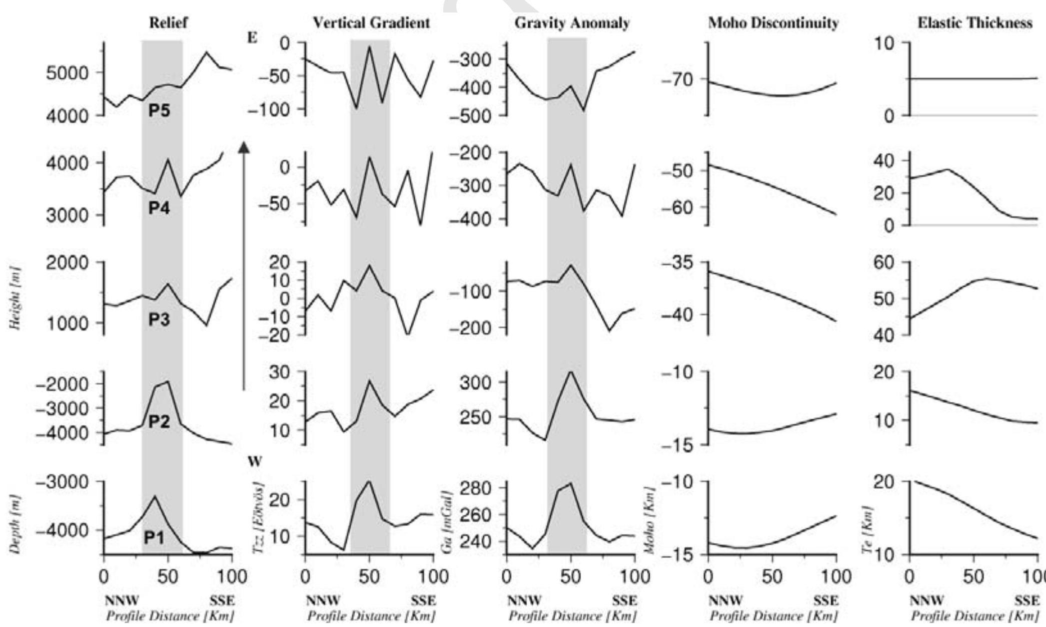

Figure E1. *Longitudinal profiles (C1, Northern profile, C2, Central profile, C3, Southern profile) at the path of the Copiapó ridge offshore and beneath the South*

America Plate, comparing topography, Tzz, Bouguer anomaly, Moho and Te (see Figure 5b for location).

Additionally, three profiles were traced in the N-NE direction along and parallel to the ridge track (for location see Fig. 5b). Profile C1 (Fig. E2, red dotted line) was traced parallel and to the north of the ridge path; Profile C2 (Fig. E2, black solid line) was traced over the Copiapó ridge and through the Ojos del Salado-San Buenaventura volcanic lineament (Fig. 5b); and the southern profile C3 was traced parallel and to the south of C2 (Fig. E2, blue dashed line). In a general analysis, profile C2 clearly shows the roughed and prominent shape of the Copiapó ridge, while the other profiles present a flat bottom bathymetry. Additionally, the *Tzz* signal reflects the ridge track (C2), and the positive effect of the flexural bulge (outer rise) (C1, C2, C3). Inland, the profile C2 shows in general a higher mean value of topography along its track.

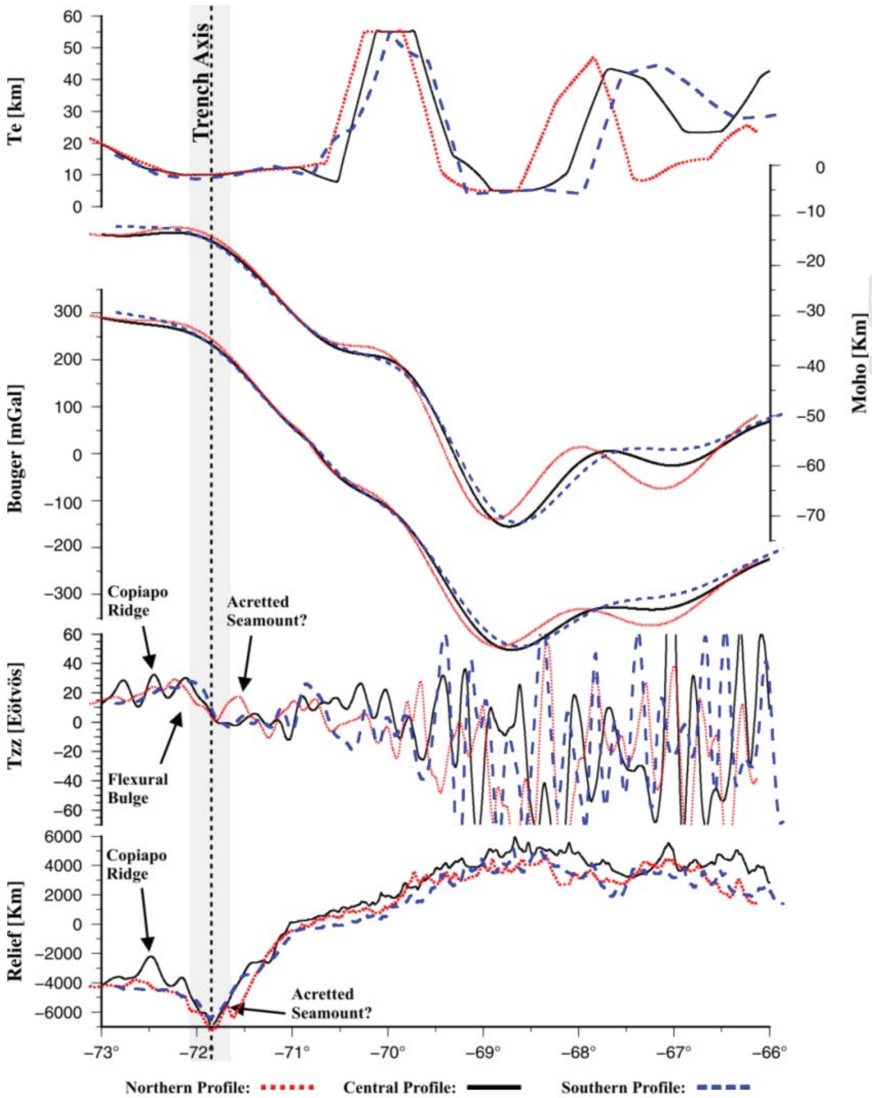

Figure E2. *2D profiles across the Copiapó ridge path comparing topography, Tzz, Bouguer anomaly and Te (see Figure 5b for location).*

Table A1: *Euler poles used in the reconstruction.*

Moving/Fix Plate	**Lon**	**Lat**	**Age(My)**	**Angle**	**Reference**
Naz./South-Am.	-98º	-54.9º	8	5.328	*DeMets et al. 2010*
Naz./Pac.	-89.75º	60.11º	10.9	-14.88	*Muller et al. 2008*

	-91.50º	64.5º	20.1	-30.70	*Muller et al. 2008*
Far./Pac.	-92.61º	73.53º	23.0	-31.08	*Muller et al. 2008*
	-110.70º	76.10º	33.1	-45.27	*Tebens and Cande, 199*
	-122.97º	82.19º	40.1	-52.24	*Muller et al. 1997*
	-160.16º	85.24º	47.9	-62.78	*Muller et al. 1997*

Table 1. *Euler poles used in the reconstruction.*

Highlights

Vertical gravity gradient show a deflection of the main Andean structures trend

Relationship between the Copiapo ridge and deformation in the upper plate

The Copiapo ridge controls the northern edge of the Chilean flat subduction zone

Leading to shallower subduction at the northern region of the Chilean flat-slab

Chilean-Pampean flat slab could be related to two simultaneous ridge collision

Moving/Fix Plate	**Lon**	**Lat**	**Age(Ma)**	**Angle**	**Reference**
Naz./South-Am.					
	-98º	-54.9º	8	5.328	DeMets et al., 2010
Naz./Pac.					
	-89.75º	60.11º	10.9	-14.88	Muller et al., 2008

	-91.50º	64.5º	20.1	-30.70	Muller et al., 2008
Far./Pac.					
	-92.61º	73.53º	23.0	-31.08	Muller et al., 2008
	-110.70º	76.10º	33.1	-45.27	Tebens and Cande, 199
	-122.97º	82.19º	40.1	-52.24	Muller et al., 1997
	-160.16º	85.24º	47.9	-62.78	Muller et al., 1997

Table 1. Euler poles used in the reconstruction.

Average difference	*0.0772 mgal*
Standard Deviation	*12.341 mgal*
Maximal value of difference	*62.021 mgal*

Table B1: *Statistical parametrs for the difference.*

Masses above sea level	ρ_s	2,670 kg/m^3
Upper crustal density	ρ_{uc}	2,700 kg/m^3
Lower crustal density	ρ_{lc}	2,900 kg/m^3
Upper mantle density	ρ_m	3,300 kg/m^3

Young modulus	E	10^{11} N/m^2
Poisson ratio	Σ	0.25

Table C1. Parameters used in the flexural modeling.